Signal Processing for In-Situ Detection of Effective Heat Pulse Probe Spacing Radius as the Basis of a Self-Calibrating Heat Pulse Probe

Nicholas J. Kinar[1], John W. Pomeroy[1], Bing Si[1,2]

5 [1]Global Institute for Water Security, Centre for Hydrology, Smart Water Systems Lab, University of Saskatchewan
[2]Department of Soil Science, College of Agriculture and Bioresources, University of Saskatchewan

Correspondence to: Nicholas J. Kinar (n.kinar@usask.ca)

Abstract. A sensor comprised of an electronic circuit and a hybrid single and dual heat pulse probe was constructed and tested along with a novel signal processing procedure to determine changes in the effective dual-probe spacing radius over the time
10 of measurement. The circuit utilized a proportional–integral–derivative (PID) controller to control heat inputs into the soil medium in lieu of a variable resistor. The system was designed for on-board signal processing and implemented USB, RS-232 and SDI-12 interfaces for Machine-to-Machine (M2M) exchange of data, thereby enabling heat inputs to be adjusted to soil conditions and data availability shortly after the time of experiment. Signal processing was introduced to provide a simplified single-probe model to determine thermal conductivity instead of reliance on late-time logarithmic curve-fitting.
15 Homomorphic and derivative filters were used with a dual-probe model to detect changes in the effective probe spacing radius over the time of experiment to compensate for physical changes in radius as well as model and experimental error. Theoretical constraints were developed for an efficient inverse of the exponential integral on an embedded system. Application of the signal processing to experiments on sand and peat improved the estimates of soil water content and bulk density compared to methods of curve-fitting nominally used for heat pulse probe experiments. Applications of the technology may be especially
20 useful for soil and environmental conditions where effective changes in probe spacing radius need to be detected and compensated over the time of experiment.

1 Introduction

The Heat Pulse Probe (HPP) is widely used to determine thermal conductivity (Abu-Hamdeh, 2001; Abu-Hamdeh and Reeder, 2000; Jin et al., 2017; Li et al., 2016; Liu et al., 2007; Ochsner and Baker, 2008; Penner, 1970; Yun and Santamarina, 2008),
25 thermal diffusivity and heat capacity (Bristow, 1998; Ham and Benson, 2004; Kluitenberg et al., 1993; Liu et al., 2007; Ochsner et al., 2001; Zhang et al., 2014) of soil. HPPs have been used to measure the thermal conductivity (Morin et al., 2010; Sturm and Johnson, 1992) and density of snow (Liu and Si, 2008); a review is presented by Kinar and Pomeroy (2015). For soils, HPP measurements provide inputs for mathematical models used to determine volumetric water content (Basinger et al., 2003; Bristow, 1998; Bristow et al., 1993; Ham and Benson, 2004; Heitman et al., 2003; Li et al., 2016; Song et al., 1998) and water
30 flux (Hopmans et al., 2002; Kamai et al., 2008; Mori et al., 2003; Wang et al., 2002). A comprehensive review of HPP sensors used to measure water flux is given by He et al. (2018). Installed into a tree trunk (Green et al., 2003) or plant stem (Miner et al., 2017), HPPs can measure sap flow rates. Multi-functional HPPs can simultaneously measure soil thermal and electrical properties to determine soil water retention and hydraulic conductivity (Bristow et al., 2001; Mori et al., 2003; Valente et al., 2006). Data from HPPs can be used to drive predictive mathematical models for water transport (Liu and Si, 2008; Saito et
35 al., 2006; Trautz et al., 2014) and snowpack evolution (Ochsner and Baker, 2008). These models are also useful for civil and geological engineering applications (Ochsner et al., 2001), as well as for prediction of runoff (Yang and Jones, 2009),

agricultural productivity (Pearsall et al., 2014; Sturm and Johnson, 1992), climate change and avalanche hazards (Morin et al., 2010).

HPPs can be broadly classified into two different types: Single Probe (SP) (De Vries, 1952; Li et al., 2016) and Dual

40   Probe (DP) (Bristow et al., 1993; Campbell et al., 1991; Ham and Benson, 2004) devices. The SP consists of a single heater needle that is inserted into the geomaterial. A temperature measurement sensor (i.e. a thermistor) placed inside of the heater needle is used to determine the change in temperature as the needle releases thermal energy. The DP consists of two needles that are inserted into the geomaterial: one of the needles functions as a heater, whereas the other needle measures the change in temperature of the geomaterial at an offset distance to the heated needle. The DP has an advantage over the SP since the

45   SP can only be used to determine thermal conductivity, whereas the DP can be used to determine thermal conductivity and diffusivity of the geomaterial (Bristow et al., 1994).

An assumption nominally made in conjunction with DP sensors is that the radius is constant during each measurement. If the DP radius changes after the probe is inserted into the geomaterial or over the time of measurement due to heating and cooling, HPP determination of thermal properties will be inaccurate (Kluitenberg et al., 1993; Mori et al., 2003). The measured

50   thermal conductivity is not sensitive to changes in DP probe spacing radius, whereas the HPP-determined heat capacity and thermal diffusivity exhibit high sensitivity to radius changes (Kluitenberg et al., 2010; Liu et al., 2007). This creates challenges in estimating the moisture content of frozen soils where thawing and freezing occur, and has required recalibration of individual probes (Zhang et al., 2011).

This paper introduces a new Self-Calibrating Heat Pulse Probe (SCHEPP) system that consists of a custom electronic

55   circuit and novel inverse models for the SP and DP. The HPP used for SCHEPP is a hybrid of the SP and DP designs. SP and DP forward models are combined and used to determine changes in the effective probe spacing radius during the time of measurement. This effective radius compensates for model error and similar to a calibrated probe spacing radius does not directly coincide with the actual probe spacing radius. Another inverse model is also introduced that allows for determination of thermal conductivity without the need for an SP model late-time approximation.

60   A Proportional-Integral-Derivative (PID) controller is used to precisely control and maintain heat inputs in lieu of a variable resistor. Circuit theory is used to determine the resistance of the Nichrome heating wire inside of the heater needle during a measurement. This eliminates the need to use a previously-measured estimate of the heater wire resistance. The heater wire resistance is directly measured over the time of an experiment.

Most HPP researchers utilized commercially available off-the-shelf (COTS) hardware (i.e. a datalogger) to collect

65   data (Bristow, 1998; Bristow et al., 1994, 2001; Kamai et al., 2008; Li et al., 2016), although recently custom electronic circuits have been proposed. Valente et al. (2006) interfaced a multi-functional soil probe to a processing circuit. Dias et al. (2013) used an NPN transistor as a heat source for a SP device. The temperature of the transistor was determined using a circuit and transistor circuit theory. Sherfy et al. (2016) used an NE555 timer circuit to control the duration of the heating pulse. Miner et al. (2017) and Ravazzani (2017) developed Arduino-based HPP sensors utilizing currently-established DP theory.

70   Liu et al. (2013), Wen et al. (2015), and Liu et al. (2016) showed that two or more thermistors placed inside the

temperature measurement needles of a DP device can be used to determine probe deflection. Multiple thermistors are required to determine probe deflection and the method cannot be used to calculate a time series of small changes in the probe spacing radius that occurs during the time of measurement when the heater needle increases in temperature.

2 Materials and Methods

2.1 Forward Models

Diagrams of the SCHEPP system HPP are shown as Fig. 1 and 2a. A loop of Nichrome wire is placed inside of a heater needle, along with a measurement thermistor. Another measurement thermistor is placed inside of a temperature-sensing needle situated at an offset distance to the heater needle. Figure 2a shows that SCHEPP uses a hybrid SP and DP device.

Assuming that the heater needle is an infinite line source in an infinite medium, the "late-time" change in temperature $\Delta\Gamma_1(t)$ of the heater probe SP device is given by Eq. 22a of Blackwell (1954):

$$\Delta\Gamma_1(t) = \frac{q}{4\pi k}\log(t) + B + \frac{1}{t}\left((C)\log(t) + D\right), \quad t > 0 \tag{1}$$

In Eq. (1) above, q is the rate of energy transferred per unit length of the probe, k is the thermal conductivity of the geomaterial, $\{B, C, D\}$ are constants and the natural logarithm is utilized. The assumption of an infinite line source in an infinite medium is valid if the heater needle has a small diameter and the geomaterial is of sufficiently large dimension to be isotropic and homogeneous throughout so that the heat pulse does not interact with dissimilar boundaries (i.e. a container in which the soil is placed) over the time of the measurement (Kluitenberg et al., 1993, 1995; Liu et al., 2007). For $t \gg r_n^2/\alpha$, where r_n is the radius of the needle and α is the thermal diffusivity of the medium, the last term in Eq. (1) can be neglected (Bristow et al., 1994; Li et al., 2016). In this paper, Eq. (1) as a forward model is taken subject to the constraint that $\Delta\Gamma_1(t) > 0$ since negative values are not physically reasonable within the context of the model.

Assuming an infinite line source in an infinite medium for a DP device, the change in temperature $\gamma_1(r,t)$ sensed at a radial distance r from the heater needle is (Kluitenberg et al., 1993):

$$\gamma_1(r,t) = \begin{cases} \Delta T_1(r,t), & t_0 < t \le t_h \\ \Delta T_2(r,t), & t > t_h \end{cases} \tag{2}$$

$$\Delta T_1(r,t) = \frac{-q}{4\pi k} E_i\left(\frac{-r^2}{4\alpha t}\right), \quad t > 0 \tag{3}$$

$$\Delta T_2(r,t) = \frac{q}{4\pi k}\left[E_i\left(\frac{-r^2}{4\alpha(t-t_h)}\right) - E_i\left(\frac{-r^2}{4\alpha t}\right)\right], \quad t > 0 \tag{4}$$

100

$$\alpha = \frac{k}{\rho c} \tag{5}$$

The thermal diffusivity of the medium is α, the density is ρ, and the specific heat capacity is c. The exponential integral function is $E_i(\ )$. The current through the Nichrome wire is turned on at time t_0 and turned off at time t_h. Therefore,

105 $t_0 < t \le t_h$ is referred to as the heating period, and $t > t_h$ as the cooling period. Calibration to determine a radius using least-squares curve-fitting will yield an effective radius that is representative of differences between the sensing system and the ideal model described above. This initial radius is referred to as $r_{initial}$ and is nominally taken as a constant.

2.2 Inverse Models

110 **2.2.1 Thermal Conductivity**

Curve-fitting using Eq. (1) can be conducted for the section of the heating curve where $t \gg r_n^2/\alpha$. However, the late-time approximation with $t \gg r_n^2/\alpha$ increases the time of measurement and necessitates that the $1/t$ term is negligible. When $t < r_n^2/\alpha$ and for suitable t such that the model of Eq. (1) is valid, the $\{k, B, C, D\}$ are difficult to directly determine using curve fitting by optimization where multiple values can be found to appropriately fit the same model of Eq. (1).

115   Given these disadvantages, this section introduces a method (the "Signal Processing SP Model") to use signal processing to reduce the time series associated with Eq. (1) to a simpler model. Least-squares curve-fitting is used with a modified version of Eq. (1) and the total SP dataset during heating. Errors introduced during the earlier time of heating are acceptably small, particularly when signal processing has modified the SP dataset as a time-domain signal and curve-fitting is used to obtain k in a least-squares fashion.

120   Equation (1) is subjected to Hadamard (point-by-point) multiplication by t to obtain

$$\Delta\Gamma_2(t) = t\left[\Delta\Gamma_1(t)\right] = \frac{qt}{4\pi k}\log(t) + Bt + (C)\log(t) + D \tag{6}$$

Geoscientific
Instrumentation
Methods and
Data Systems
Discussions

Open Access

The Hadamard multiplication to produce Eq. (6) is a type of homodyning process where later-time values of $\Delta\Gamma_1(t)$ are

125 assigned greater-magnitude weights than earlier-time values. Taking the numerical time derivative is similar to application of a high-pass filter (Hamming, 1983; pg. 118). The resulting equation is:

$$\Delta\Gamma_3(t) = \frac{d}{dt}\Delta\Gamma_2(t) = \frac{q}{4\pi k}\left[\log(t)+1\right]+B+\frac{C}{t} \tag{7}$$

130 Homodyning again by t yields:

$$\Delta\Gamma_4(t) = t\left[\Delta\Gamma_3(t)\right] = \frac{qt}{4\pi k}\left[\log(t)+1\right]+Bt+C \tag{8}$$

Taking the numerical time derivative again:

$$\Delta\Gamma_5(t) = \frac{d}{dt}\left[\Delta\Gamma_4(t)\right] = \frac{q}{4\pi k}\left[\log(t)+2\right]+B \tag{9}$$

135

To reduce noise associated with the derivative operation when working with actual data, a Butterworth lowpass filter with zero-phase filtering and a cutoff frequency of 0.3 Hz is applied to the numerical sequence associated with Eq. (9). The cutoff frequency was chosen to ensure stability of the inverse model within the context of the data used for the experiments reported by this paper. Given a known q, curve-fitting is applied to the filtered sequence associated with Eq. (9) to determine k

140 without the need to also determine $\{C, D\}$ at time $t < r_n^2/\alpha$ where the model of Eq. (1) is still valid. Once the thermal conductivity k is determined by the signal processing, curve-fitting using Eq. (1) with a starting value of the determined thermal conductivity is used to estimate parameters for application of the SP forward model.

      The "Late-Time SP Model" is used for comparison with the Signal Processing SP Model described above. A linear section of the $\Delta\Gamma_1(t)-\log(t)$ curve is identified as the time t_d that is 1 s after the time when the second numerical derivative

145 of the $\Delta\Gamma_1(t)-\log(t)$ curve is approximately equal to zero. The time t_d is identified using a signal processing zero-crossing detector and the 1s delay is introduced to ensure that the curve is approximately linear. Curve-fitting using Eq. (1) with $C = D = 0$ is then used to determine k from the linear section of the $\Delta\Gamma_1(t)-\log(t)$ curve. This is a nominal curve-fitting method (Li et al., 2016) that is implemented in the context of this paper.

150 2.2.2 Dual Probe and Variable Radius

The inverse model described in this section uses signal processing to determine $r(t)$ as an effective radius that changes over the time of heating and cooling to compensate for model error and physical changes in the probe spacing. A numerical value for $r_{initial}$ is required as an estimate of the initial probe spacing radius. Changes in the effective probe spacing $r(t)$ are determined over time and used to obtain an α that is representative of these changes. This is the "Signal Processing DP"
155 model.

The thermal conductivity k is determined using a measured q, and the inverse signal processing model presented in Section 2.2.1 for the SP. The thermal conductivity is not directly determined from the DP model using curve-fitting since the effective radius $r(t)$ can change over time.

The k is used with a known q to algebraically remove the $q/4\pi k$ term from Eq. (2) to obtain $\gamma_2(r(t),t)$ as an
160 expression written only in terms of $E_i(\ )$. The inverse of the exponential integral is determined using the procedure in Appendix A suitable for an embedded system.

From the inverse, we determine:

$$\gamma_3(r(t),t) = \frac{-(r(t))^2}{4\alpha} \tag{10}$$

165
$$\gamma_4(r(t),t) = -\gamma_3(r(t),t) = \frac{(r(t))^2}{4\alpha} \tag{11}$$

The square root function transforms Eq. (11) to Eq. (12) below. To ensure application of the square root function with real numbers, the computer implementation must ensure $\gamma_4(r(t),t) > 0$.

170
$$\gamma_5(r(t),t) = \left[\gamma_4(r(t),t)\right]^{1/2} = \frac{r(t)}{2\alpha^{1/2}} \tag{12}$$

Taking the logarithm of Eq. (12) results in Eq. (13) below. Applied to each element of the corresponding sequence, this operation is analogous to Homomorphic filtering (Oppenheim et al., 1976).

$$\gamma_6(r(t),t) = \log(\gamma_5(r(t),t)) = \log(r(t)) - \log(2\alpha^{1/2}) \tag{13}$$

175

Taking the time derivative of Eq. (13) is once again similar to the application of a high-pass filter that suppresses the constant $\log\left(2\alpha^{1/2}\right)$ term. When Eq. (14) is expressed as a discrete sequence sampled at a frequency of f_s the derivative is approximated using a backward-difference method (Eq. (15)).

180

$$\gamma_7\left(r(t),t\right) = \frac{d}{dt}\gamma_6\left(r(t),t\right) = \frac{d}{dt}\log\left(r(t)\right) \tag{14}$$

$$\frac{d}{dt}\gamma\left(r(t),t\right) \approx \frac{a_{i-1} - a_i}{\Delta t} \tag{15}$$

185   In Eq. (15) above $a_i = \log\left(r(t_i)\right)$, where the index i denotes the element of a discrete sequence and Δt is the timestep calculated by $\Delta t = 1/f_s$. To reduce numerical error at small time t values, the inverse model described in this section is applied with a timestep Δt such that the numerical inverse of $E_i(x)$ can be successfully computed (Section 2.5).

       Solution of Eq. (15) requires a boundary condition $a_b = \log\left(r(t_{initial})\right)$, where $t_{initial}$ is the time at which the probe spacing radius is $r_{initial}$. For application to actual data, we assume that the probe spacing is the calibrated $r_{initial}$ at 190 $t_{initial} = t_p + t_a$ where t_p is the time where the curve associated with $\gamma_1(r,t)$ is at a maximum and t_a is an additional time delay that compensates for a non-ideal system. This is a similar idea to the temperature maximum method (Bristow et al., 2001) where the calibrated $r_{initial}$ is used at the time of peak temperature change. For the system used in the context of this study, $t_a = 2$ s as an integer-valued time delay to coincide with the time duration of moving-average windows (Section 2.5). The input data is trimmed appropriately. This selection of boundary condition is supported by tests on actual soil performed in this 195   paper and a sensitivity analysis that justifies the selection of the additional time t_a (Section 3.3).

       After $r(t)$ is determined, the α as a constant is determined by taking the average of $\gamma_8\left(r(t),t\right)$ over time. Evaluation of Eq. (16) will thereby yield a curve that is nominally a straight line with a slope that is approximately zero when α is approximately constant over the time of heating and cooling. The $r(t)$ is an effective radius that is also affected by temperature drift and deviation of the physical system from an ideal model. Since $r(t)$ is an effective radius, it will not 200   directly coincide with an actual probe spacing radius.

$$\gamma_8\left(r(t),t\right) = \frac{\left(r(t)\right)^2}{4\gamma_4\left(r(t),t\right)} \approx \alpha \tag{16}$$

2.3 Measurement of Soil Water Content and Density

The heat capacity k and thermal diffusivity α are determined using an inverse model as described in the previous sections of this paper. Neglecting the contribution of air, the volumetric heat capacity of soil C_h is calculated by (Kluitenberg, 2002):

$$C_h = \theta_m C_m + \theta_o C_o + \theta_w C_w \tag{17}$$

Re-arranging Eq. (17) and solving for volumetric water content:

$$\theta_w = \frac{1}{C_w}\left[C_h - \left(\theta_m C_m + \theta_o C_o\right)\right] \tag{18}$$

$$C_h = k / \alpha$$

$$C_m = c_m \rho_m$$

$$C_o = c_o \rho_o$$

In the equations above, $\{C_m, C_o, C_w\}$ are the volumetric heat capacities of mineral content, organic content, and water; $\{\theta_m, \theta_o, \theta_w\}$ are the associated volume fractions; and C_h is the total volumetric heat capacity of the soil. The $\{c_m, c_o\}$ are the specific heat capacities of the mineral and organic content and the $\{\rho_m, \rho_o\}$ are the associated densities. Experiments where numerical values of $\theta_w < 0$ or $\theta_w > 1$ are not valid and indicate improper contact between the probe and the soil medium. The θ_w is numerically constrained to be within this range. The mineral content of the soil θ_m is known and the organic content θ_o can be easily determined from laboratory testing or an organic carbon soil map of a geographic area. For implementation using a microcontroller, θ_m and θ_o are stored in flash (non-volatile) memory and these values change based on the geographic location of the soil. The density of the soil is determined by volume fractions:

$$\rho = \theta_m \rho_m + \theta_o \rho_o + \theta_w \rho_w \tag{19}$$

In the equations above, the unknown particle densities and heat capacities are known values.

235 **2.4 Circuit Theory and PID Control**

Figure 1 shows a conceptual block diagram of the system. Thermistors in half-bridge configurations are used to determine the temperatures of HPP needles.

The heat input into the soil by the heater probe is:

240
$$P = I^2 R_w \tag{20}$$

$$q = \frac{P}{\ell} \tag{21}$$

In the above Eq. (20) and Eq. (21), the electrical power is P, the total resistance of the Nichrome heater wire is R_w, and ℓ is

245 the length of the heater needle. Given a measured voltage drop ΔE over a four-terminal Kelvin sense resistor with known resistance R_s, the current though the heater wire is calculated using Ohm's law:

$$I = \frac{\Delta E}{R_s} \tag{22}$$

For a current I through the heater wire and sense resistor, the output voltage is measured as E_{kn} by an analog-to-digital converter (Fig. 1). Using Kirchhoff's voltage law for this circuit, the resistance R_w of the Nichrome wire is determined at

250 each sampling timestep by:

$$R_w = \frac{E_{kn} - \Delta E}{I} \tag{23}$$

Geoscientific
Instrumentation
Methods and
Data Systems
Discussions
Open Access
EGU

To set a constant q, a proportional-integral-derivative (PID) controller (Ang et al., 2005) is utilized. The variable

255   voltage source is adjusted at each discrete timestep by a digital-to-analog-converter (DAC). Since ΔE and E_{kn} are measured

at each discrete timestep at a sampling rate of f_s, Eq. (20) to Eq. (23) are used with the feedback loop shown in Fig. 1 to

ensure that the q remains close to a set-point value during the time of experiment. The use of the PID controller requires a

higher sampling rate f_s than a nominal HPP experiment to adjust the output q. The PID controller thereby ensures that the

soil can heat up in a controlled fashion and considers resistance changes in the Nichrome wire in lieu of using an assumed

260   resistance. Figure 2a is a block diagram indicating how the system incorporates a microcontroller and communication

interfaces.

2.5 Determination of Temperature Change Curves

265   The sampled temperature inside the heater needle is denoted as $\Gamma(t)$ and the sampled temperature inside the second needle at

an offset distance from the heater needle is denoted as $T(t)$. The sampled temperatures $\Gamma(t)$ and $T(t)$ are lowpass filtered

using a 5th order Butterworth filter with a cutoff frequency of 10 Hz applied as a zero-phase filter to reduce noise. The

Butterworth filter was chosen since it is maximally-flat in the passband and the zero-phase filtering ensures that time shifts are

minimized to ensure accurate application of the inverse models described in this paper using the collected data.

270   For the DP model calibration to find an initial r_0 using curve-fitting, the sampled temperatures are processed by a

moving-average filter over 1 s windows to further reduce noise before curve-fitting. Alternately, for the DP inverse model

(Section 2.2.2), a moving-average filter is used to obtain an equivalent sampling rate of 12 Hz to ensure that the $E_i(x)$ inverse

can be accurately computed using floating-point number representations.

The respective averaged initial temperatures of the needles before heating are determined as Γ_{av} and T_{av}. Therefore,

275   the temperature changes are calculated as $\Delta\Gamma(t)=\Gamma(t)-\Gamma_{av}$ and $\Delta T(t)=T(t)-T_{av}$ after application of any initial filtering.

The temperature changes are used for application of inverse models related to Eq. (1) and (2).

2.6 Determination of Heat Inputs

280

Heat inputs into the soil are determined during the time of experiment and calculated using

Eq. (21). When the current is applied and travels through the heater wire, there is a short time delay ($\ll 1$ s) before the

setpoint q is attained when the heater needle increases in temperature. The interval of the time series for a constant calculated

q during the time of experiment is determined using a step detection algorithm (Carter et al., 2008) based on the Student t-
285 test (Ebdon, 1991; pp. 61-64) with a null hypothesis at a significance level of 1% and a window size of 31 elements. The
significance level and window size are dependent on the implementation of the sampling system and are thereby chosen to
detect the step within the context of this experiment. To find an estimate of a constant value of q, the time series is averaged
over the plateau of the step. The plateau of the step is found by application of a sliding mean filter with a concomitant window
size of 31 elements applied to a binary sequence created by mapping non-rejection of the null hypothesis to binary 0 and
290 rejection of the null hypothesis to binary 1. The plateau is coincident with a sequence of zeros away from the edges of the
step. The edges of the step are indicated by non-zero elements in this sequence surrounded by zeros. The window size is
appropriate for the sampling system described in the context of this paper.

2.7. Apparatus

295 A custom electronic circuit board was designed and constructed for the SCHEPP system (Fig. 2a, b). The circuit board was
placed into an enclosure box and connected to the HPP by a cable and mating circular connectors. The HPP body was epoxied
into a circular hole cut in the bottom of a cylindrical polyvinyl chloride (PVC) container of 10.0 cm diameter and 10.5 cm
height that held $825\ \mathrm{cm}^3$ of soil. The HPP needles thereby protruded into the soil column formed by the PVC container (Fig.
2c).

300   Figure 1 and Fig. 2a graphically show the different subsystems of the PCB (Fig. 2b). In the Analog Front End (AFE),
a two-channel 24-bit ADC with a precision 10k (0.01%, ±5ppm/°C) resistor half-bridge for each channel and a 2.5V voltage
reference (2 ppm/°C, ±0.02% voltage error) was used to determine the resistance of the thermistors inside of each needle. The
resistance of a thermistor was related to temperature by the Steinhart–Hart equation (Steinhart and Hart, 1968).

        The variable voltage source was constructed from a DC-DC switcher for efficiency and thereby reduced power
305 consumption in lieu of a linear regulator. The DC-DC switcher could be turned off for an output voltage of 0V or turned on
and adjusted from ~0.49V to ~8.965V using a DAC that injected current into the feedback loop of the switcher. With design
criteria heater needle length of $\ell = 3.0\ \mathrm{cm}$ and a Nichrome wire resistance of $R_w \approx 34\ \Omega$, the heater output was limited by
software to be within the range of $q \approx 0.24\ \mathrm{W\ m}^{-1}$ to $q \approx 79\ \mathrm{W\ m}^{-1}$. The precision sense resistor was chosen as $R_s = 0.01\Omega$
(0.1%, ±15ppm/°C) to reduce the voltage drop over this circuit element and to ensure that the output voltage could be accurately
310 adjusted. This resistance is smaller than the $1\ \Omega$ current sense resistor nominally used in other HPP experiments (Bristow et
al., 1994; Li et al., 2016; Liu and Si, 2011, 2008; Valente et al., 2006; Zhang et al., 2011). Moreover, the precision sense
resistor had a Kelvin terminal connection for precision and was physically large to reduce self-heating by current flow. The
voltage drop over a sense resistor was determined by a precision difference amplifier and a 16-bit ADC, allowing for a 1 LSB
step size of $2.5\mu\mathrm{V}$. The output voltage E_{kn} (Fig. 1) was also measured by a 16-bit ADC and amplifier resulting in a 1 LSB

Geoscientific
Instrumentation
Methods and
Data Systems
Discussions
Open Access
EGU

315   step size of 1.25mV.

A 32-bit microcontroller with a system clock of 300 MHz was used to control the HPP experiment and perform floating-point calculations (Fig. 2a). The microcontroller sampled all ADCs in the system at $f_s = 120\,\text{Hz}$. The DAC used to control the output voltage was also updated at the same sampling rate with the PID controller output. The 120 Hz sampling rate enabled functioning of the PID controller feedback loop and allowed for digital filtering for signal processing.

320   The microcontroller had an integrated USB transceiver for communication with a computer. RS-232 and SDI-12 interfaces were also integrated into the system for communication with a computer or datalogger as Machine-to-Machine (M2M) interfaces. SDRAM stored data from the experiment and provided temporary memory for heap allocation of arrays and data structures. Code for the microcontroller was written in the C programming language.

A command-line serial port interface permitted changing the duration of the experiment, set-point q value, and the

325   time of heating. For each experiment, the microcontroller monitored the maximum temperature rise at the heater needle and terminated the experiment if the temperature rise exceeded the maximum operating temperature of the thermistors.

The mechanical construction and design of the HPP used for this paper has been reported and rationalized in other papers (Li et al., 2016; Liu and Si, 2008, 2010). The needles of length $\ell = 3.0\,\text{cm}$ were constructed from stainless-steel tubing (1.28 mm OD and 0.84 mm ID) and filled with thermally-conductive epoxy. The sense thermistor was placed in the

330   geometric middle of each needle to prevent edge effects associated with heat conduction and the needles were filled with thermal epoxy (Saito et al., 2007). The nominal spacing between the heater needle and the sense needle was $6\,\text{mm}$. During laboratory testing of SCHEPP (Fig. 2c, d), the experiment was initiated by a laptop computer connected to the circuit's USB port and communication was conducted over the USB interface.

335

2.8 Data Collection

Following Campbell et al. (1991), calibration was conducted to find $r_{initial}$ using a 5 g/L agar gel solution. The thermal conductivity k of the agar gel was taken to be the same as the thermal conductivity of water (Saito et al., 2007). Reported

340   values for thermal conductivity (Ramires et al., 1995) and heat capacity (Wagner and Pruß, 2002) of water were used.

For all experiments, the temperature of the probe needles was measured for 1 s at a sampling rate of $f_s = 120\,\text{Hz}$ before electrical current was applied to the Nichrome wire. This initial temperature measurement for each trial was averaged over the 1 s period.

The agar gel was washed out using distilled water and the cylindrical container was packed with soil. Two types of

345   soil were used for the HPP tests: sand and peat. These soils are indicative of the physical extent of soil thermal properties. The soils were collected from field sites near Fort McMurray, Alberta. The sand contained small amounts of bitumen as representative of the Alberta Oil Sands area. Two independent laboratory analyses with incineration at 1100°C were conducted

on the sand, finding the total carbon content to range between a mean of 0.44% and 0.75% by mass. The soil properties are summarized in Table 1.

350   The water content for the sand was chosen so that the sand was saturated, whereas the water content for the peat was chosen so that the soil would remain as wet as possible (Table 1). Due to the absorbent characteristics of the peat soil, it was not possible during the time of the laboratory experiment to completely saturate the pore spaces of the soil column. However, the volumetric water content θ for both soils was chosen to ensure adequate contact between the probe and the soil and to also reduce air gaps that can increase thermal contact resistance and decrease accuracy of the measurement (Liu and Si, 2010).

355 Since the soil dried out over the time of multiple experiments, some additional water was added between successive days to ensure that the volumetric water content θ was close to the target value. Between trials, the top of the container was covered with a cap to reduce evaporation of water from the soil. Changes in water content occurred over the time of the experiment due to evaporation since the cap did not create a hermetic seal between the top of the container and the soil column. Table 1 shows quantities used for application of HPP forward and inverse models to peat and sand.

360   Experiment sampling durations, q heat inputs, and heat durations are summarized in Table 2. Trial numbers of each experiment refers to groups of experiments conducted temporally close together.

    The heat pulse strength and time of heating were chosen to minimize interaction of the heat pulse with the container boundaries. Due to the short time span over which each experiment was conducted in a laboratory setting, explicit correction was not applied for changes in ambient temperature (Young et al., 2008; Zhang et al., 2014). Between each experiment, the

365 temperature of the soil column returned to a level that approximated the initial temperature before the probe was heated again for the next trial. All experiments were conducted at room temperature (~20°C).

    Numerical comparisons were made using Root Mean Squared Difference (RMSD) and Mean Bias (MB). The RMSD indicates the overall differences between two datasets:

$$\mathrm{RMSD} = \left(\frac{1}{N} \sum_{i=1}^{N} \left(x_i - \hat{x}_i \right)^2 \right)^{1/2}$$

370

The quantity determined by a signal processing model is given by x_i and the measured value for comparison is $\hat{x}_i$. The number of comparisons is N.

    The Mean Bias (MB) indicates whether the model under-predicts or over-predicts relative to the observations. The

375 MB is defined as:

$$\mathrm{MB} = \frac{1}{N} \sum_{i=1}^{N} \left(x_i - \hat{x}_i \right)$$

3. Results

3.1 Synthetic Experiments

Synthetic heating curves were constructed using Eq. (1) and Eq. (2) to serve as a forward model and provide a test of the signal processing. The SP and DP curves are shown as Fig. 3 and Fig. 4 and were generated using the model inputs given in Table 3. For the DP, the assumed change in probe spacing radius is shown for a linear increase (Fig. 4b), decrease (Fig. 4e) and Brownian random walk scaled so that the numerical values are between a starting and ending radius (Fig. 4h).

The time-variable radius is $r(t)$ and the associated curve is shown on the plots as a "DP Variable Radius." The "DP Fixed Radius" curve is calculated using the first element of the $r(t)$ used for a particular "DP Variable Radius" curve. The fixed radius is taken to be constant over the time of heating and cooling.

For the SP, Fig. 3a shows the forward model and the reconstruction of the forward model by the inverse model proposed in Section 2.2.1. The numerical difference between the forward and inverse models is shown by Fig. 3b and is on the order of 1×10^{-7}. This difference occurs due to discretization of the numerical derivatives and floating-point round-off error from the homodyning process. The simplified model given by $\Delta\Gamma_5(t)$ is shown by Fig. 3c and demonstrates the reduction of terms from the original model (Eq. (1)). Fig. 3d is the numerical difference between the forward and inverse models associated with $\Delta\Gamma_5(t)$. The numerical difference remains small over the time of heating.

Figure 4 demonstrates the heating and cooling curves for a DP model with fixed radius and variable radius. The assumed time-variable radius $r(t)$ is given along with application of the inverse model proposed in Section 2.2.2. The first row of Fig. 4 (a, b, c) is for a linear increase; the second row of Fig. 4 (d, e, f) is for a linear decrease; and the third row of Fig. 4 (g, h, i) is for the Brownian random walk. The difference between the forward and inverse models is on the order of 1×10^{-15} for all changes in probe spacing radius (Fig. 4c-i), indicating that for a synthetic model the error is mostly associated with floating point calculations and that the inverse model is accurate.

3.2. Soil Data

Since the "Signal Processing SP" and "Signal Processing DP" models are applied together, hereafter these will be referred to as the "Signal Processing SP and DP" model. The "Late-Time SP Model" is described in Section 2.2.1. The "Heating and Cooling DP" model refers to the nominal curve-fitting using Eq. (2).

Figure 5 provides an example of the models applied to sand (Table 4). The peak time corresponding to $t_p + t_a$ is

indicated as a vertical line on Fig. 5b. Changes in effective radius $r(t)$ determined by signal processing are shown as Fig. 5c. The rapid fluctuations in the effective radius $r(t)$ occur due to temperature drift, model and experimental error. The signal processing thereby compensates for these effects using $r(t)$ as an effective radius. Table 4 shows that the quantities found

410 using all models have the same orders of magnitude and indicates that the Signal Processing SP and DP model is more accurate than the Heating and Cooling DP model as compared to the gravimetric values used for the laboratory experiment.

Figure 6 shows the Signal Processing SP and DP model applied to peat (Table 5). Compared to the sand example given above, the thermal conductivity k and diffusivity α are lower for the peat demonstrating that the peat takes longer to warm up during the time of experiment. The heating and cooling curves are thereby distinctively different between sand and

415 peat. However, in the same manner as the sand example, the quantities found using all models are of similar orders of magnitude. Fig. 6c shows that there are fewer rapid fluctuations in the effective radius $r(t)$ determined for peat as compared to sand. Moreover, the change in effective radius is less pronounced for peat as compared to sand due to smaller temperature drift associated with lower k and α. Also, in a similar fashion to sand, the PD and numerical difference demonstrates that the signal processing models introduced in this paper are more accurate than the nominal models.

420 Figure 7 shows the thermal conductivity k and diffusivity α for the sand and peat determined for the experimental trials. For the sand, the nominal Heating and Cooling DP model provides estimates of k that are mostly higher than the Signal Processing SP and Late-Time SP models. The Late-Time SP model provides estimates of k that are intermediate between the other two models. The Signal Processing SP model produces the lowest estimates of k. However, the estimates of k made by all three models are the same orders of magnitude and remain relatively constant over experiments conducted on each soil

425 type. The thermal diffusivity estimates provided by the Heating and Cooling DP model are slightly higher than the estimates provided by the Signal Processing SP and DP model for sand (Fig. 7c), whereas for peat (Fig. 7d) the thermal diffusivity for both models is approximately similar.

Results corresponding to Fig. 7 to Fig. 8 are shown by Tables 6-7. These tables show RMSD, MB, PD and the results of these calculations are discussed below.

430 Fig. 8 shows the determined values of water content θ_w and density ρ. Overall, for the sand and peat experiments, the nominal Heating and Cooling DP model has a higher magnitude RMSD, MB and PD compared to the Signal Processing SP and DP model introduced in this paper, indicating that determination of the effective $r(t)$ by signal processing improves estimates of θ_w and ρ.

For all sand experiments, the Signal Processing SP and DP model reduces the θ_w RMSD by 0.10 (10%), the MB by

435 0.33 (33%), and the PD by 4.2% compared to the nominal Heating and Cooling DP model. For all peat experiments, the corresponding reduction for θ_w is 0.07 (7%) for the RMSD, 0.41 (41%) for the MB, and 12.3% for the PD.

For the density ρ of sand, the Signal Processing SP and DP model reduces the RMSD by 102 kg m^{-3}, the MB by 338 kg m^{-3}, and the PD by 0.85%. For the density ρ of peat, the Signal Processing SP and DP model reduces the RMSD by 94 kg m^{-3}, the MB by 407 kg m^{-3}, and the PD by 5.1%.

440   For experiment identifiers A, B, C, D associated with sand, the RMSD, MB and PD magnitudes are lowest for θ_w determined from the Signal Processing SP and DP model compared to the nominal Heating and Cooling DP model. The RMSD, MB and PD magnitudes are also lower for most sand estimates of ρ other than experiment identifier D, where the RMSD and MB magnitudes are larger than magnitudes associated with the nominal Heating and Cooling DP model. The heat pulse strength and duration was of greater magnitude for experiment identifier D, but since ρ is being calculated as a function

445   of θ_w this indicates a change in soil constituents (cf. Equation (19)) in the vicinity of the probe for experiment identifier D and demonstrates sensitivity of the signal processing to this change.

        An increase in water content is apparent for experiment identifiers E to G associated with peat. The increase in water content occurred since the HPP experiments were initially conducted less than an hour after water was added to the soil column. Since the soil column was opaque, the infiltration of water in the column and the associated wetting front could not be tracked

450   and thereby localized volumes of water surrounding the HPP caused a rise in water content. Since the rise is consistent and shown by the Heating and Cooling DP model as well as the Signal Processing SP and DP model for θ_w and ρ (Fig. 8b, d), this indicates that both models are in physical agreement. Lower RMSD, MB and PD values for the Signal Processing SP and DP model indicates that the signal processing introduced in this paper also improves estimates of θ_w and ρ when the water content changes during the time interval of experiment identifier E.

455   For experiment identifiers F and G, the determined θ_w and ρ remains approximately constant over time for peat. Compared to experiment identifier E, a reduction in water content has occurred due to infiltration over time and some loss of water due to evaporation. For these experiments, the RMSD, MB and PD is lower for the Signal Processing SP and DP model compared to the Heating and Cooling DP model.

460   **3.3 Sensitivity Analysis**

To identify the effects of model parameters on the RMSD and MB of model outputs θ_w and ρ, a sensitivity analysis (Fig. 9 to Fig. 10) was conducted over all data collected. The sensitivity analysis utilized the OAT approach, where one variable at a time is changed whereas the other model inputs are held constant. Overall, for a range of nominal model inputs, Fig. 9 to Fig. 10 demonstrate that the signal processing associated with the Signal Processing SD and DP model reduces the RMSD and MB

465   compared to the nominal Heating and Cooling DP model. This also indicates that the signal processing method produces more accurate estimates than the curve-fitting models nominally used for heat pulse probe experiments.

Geoscientific
Instrumentation
Methods and
Data Systems
Discussions

Open Access

EGU

For all models and soils used to determine θ_w and ρ, the RMSD and MB is lowest when the initial radius $r_{initial}$ is close to the calibrated value, indicating the importance of calibration for all models. If the $r_{initial}$ is underpredicted, the MB indicates an overprediction of θ_w and ρ, whereas an overprediction of r_0 indicates an underprediction of θ_w and ρ.

470   For sand θ_w, an organic content $\theta_o < 0.1$ produces the lowest magnitude RMSD and MB, whereas for peat θ_w, an organic content close to $\theta_o \approx 0.40$ produces the lowest magnitude RMSD and MB. This physically approximates the composition of the sand and peat soils used for these experiments. The MB for sand and peat indicates a model overprediction for θ_o values lower than these thresholds and a model underprediction for θ_o values higher than these thresholds. A similar effect is also shown for the mineral content θ_m, with $\theta_m \approx 0.60$ resulting in the lowest magnitude RMSD and MB for sand.

475   For peat, $\theta_m \approx 0.15$ results in the lowest magnitude RMSD and MB.

For sand θ_w the time delay $t_a \approx 1.5$ s is a good assumption to provide the lowest values of RMSD and MB for the Signal Processing SD and DP model for both sand and peat. For peat ρ the time delay $t_a \approx 0$ s. The time delay t_a is not a parameter for the nominal Heating and Cooling DP model and a sensitivity analysis is not conducted for t_a when using this model. Applied to peat, the Signal Processing SD and DP model is relatively insensitive to the time delay t_a due to the lower thermal conductivity k and diffusivity α relative to sand that dampens changes in the effective radius $r(t)$ as determined by signal processing.

In the context of the sensitivity analysis, as θ_o increases for sand, the RMSD and MB related to ρ also increases. For peat, a concomitant increase in θ_o is associated with an increase in the RMSD and MB, indicating that for ρ it is not possible to calibrate for θ_o and an approximation of θ_o must be known for model application within the context of these experiments. A mineral content of $\theta_m \approx 0.55$ for sand produces the lowest RMSD and MB related to related to ρ. As θ_m increases for peat, the RMSD and MB also increases, indicating that for ρ it is once again not possible to calibrate for θ_m and an approximation must be utilized.

4. Conclusions

- A novel circuit was designed and tested using a hybrid SP and DP Heat Pulse Probe (HPP) design. The circuit utilized a PID controller to precisely control the heat input into the soil. In lieu of a variable resistor, this enabled the heat input q to be changed by a computer or a datalogger. When deployed at a remote or inaccessible field site, the HPP heat input can be set to a given value using the communication interfaces. This enables the heat input to be appropriately selected for soil type.

495
- Instead of using a $1\,\Omega$ sense resistor to infer heat inputs into the soil, the circuit used a resistor with a $0.01\,\Omega$ nominal resistance. This reduced the voltage drop across the sense resistor and still allowed for the current through the Nichrome wire to be adequately determined during the time of experiment, although a differential amplifier was required to detect the voltage difference before digitization by an ADC.

500
- A sampling rate of 120 Hz was required for application of the PID controller and theory associated with signal processing related to a hybrid SP and DP Heat Pulse Probe. The higher sampling rate allowed for digital filtering to be applied.

- Signal processing was used to determine thermal conductivity using a SP model that did not rely on a late-time SP
505
  approximation. A DP model was used to determine changes in the effective DP probe spacing radius.

- The DP and SP signal processing models introduced in this paper improved overall estimates of soil water content θ_w and bulk soil density ρ for sand and peat soils, indicating that detection of effective changes in the probe spacing radius using signal processing is useful to correct for model error and physical changes in the probe spacing. This
510
  improvement is associated with standard HP and DP probes that are used together in a novel fashion along with signal processing.

- Further research is required to test the signal processing models introduced in this paper and to compare the estimates of soil water content θ_w and bulk soil density ρ to estimates made using other measurement systems and
515
  technologies. The potential exists for the theory described in this paper to be extended for application to frozen soils, where the heat input q can cause phase changes in the soil that are associated with changes in the effective probe spacing radius $r(t)$.

5. Code Availability

520 The computer code and data used to produce the figures and numerical results in this paper can be downloaded from Github
(https://github.com/smartwaterlab)   and   is   also   available   as   a   link   from   Figshare
(https://www.doi.org/10.6084/m9.figshare.11372181).

525

6. Data Availability

The data from the experiments described in this paper can be downloaded from the Figshare data repository (https://www.doi.org/10.6084/m9.figshare.11371455).

530 ## 7. Appendix A

To efficiently obtain the inverse of $E_i(x)$, endpoints for a search interval need to be appropriately selected, particularly when the inverse model runs on an embedded resource-constrained microcontroller. To ensure numerical continuity and accuracy between the forward and inverse models, the same $E_i(x)$ function is used in the inverse of $E_i(x)$ in lieu of alternative numerical approximations.

535   Take $E_1(x) = -E_i(-x)$, where $E_1(x) = E_n(x)$ with $n = 1$. Let $x > 0$ and we need to show:

$$-\frac{1}{x^{1/2}} < E_1(x) < \frac{1}{x^{1/2}} \qquad (A.1)$$

Using 5.1.20 of Abramowitz and Stegun (1964), we need to show that with $x > 0$:

540

$$-\frac{1}{x^{1/2}} < \frac{1}{2}\exp(-x)\log\left(1+\frac{2}{x}\right) < E_1(x) < \exp(-x)\log\left(1+\frac{1}{x}\right) < \frac{1}{x^{1/2}}$$

Since $\exp(-x) > 0$ and $\log\left(1+\frac{2}{x}\right) > 0$ as $x \to \infty$, then $\frac{1}{2}\exp(-x)\log\left(1+\frac{2}{x}\right) > 0$ as $x \to \infty$. Therefore $-\frac{1}{x^{1/2}} < \frac{1}{2}\exp(-x)\log\left(1+\frac{2}{x}\right)$. We next show

545

$$\exp(-x)\log\left(1+\frac{1}{x}\right) < \frac{1}{x^{1/2}}$$

Algebraic re-arrangement yields

$$\frac{1}{2}\log(x) + \log\left(\log\left(1+\frac{1}{x}\right)\right) < x$$

550

Since $x > 0$, we need to show

$$\frac{1}{2}\log(x) + \log\left(\log\left(1+\frac{1}{x}\right)\right) < 0$$

555

By algebraic re-arrangement, we find

$$1 + \frac{1}{x} < \exp\left(\frac{1}{x^{1/2}}\right)$$

560 The RHS can be replaced by a power series representation

$$1 + \frac{1}{x} < \sum_{i=0}^{\infty} \frac{x^{-i/2}}{i!}$$

The proof proceeds by contradiction and shows that the inequality holds. We assume

$$1 + \frac{1}{x} \geq 1 + \frac{1}{x^{1/2}} + \cdots$$

565

However, this is a contradiction, so inequality (A.1) holds.

From inequality (A.1), the search interval for $E_i(x)$ is $\left[-1/\left(E_i(x)\right)^2, 0\right)$ for $x < 0$. The inverse of $E_i(x)$ is computed using Golden-section search (Kiefer, 1953) on the bounded interval.

The following shows how endpoints of the search interval for the inverse are selected for the cooling section of the

570 DP curve using the result given above. Without the $q/(4\pi k)$ term, Eq. (4) is of the form:

$$f(x, y) = f(h) = E_i(-x) - E_i(-y) \tag{A.2}$$

Let $x = h/(t - t_h)$ and $y = h/t$, where $h = (r(t))^2/(4\alpha)$ and $x > 0$ and $y > 0$. Eq. (A.2) can be re-written as:

575

$$f(h) = f(x, y) = -E_1(x) + E_1(y)$$

From the above and inequality (A.1):

580

$$\frac{-1}{x^{1/2}} - \frac{1}{y^{1/2}} < -E_1(x) + E_1(y) < \frac{1}{x^{1/2}} + \frac{1}{y^{1/2}}$$

Algebraic manipulation yields the following search interval for $t > t_h$:

585

$$0 < h < (t - t_h) \left[\frac{1+z}{z} \frac{1}{-E_1(x) + E_1(y)} \right]^2 \qquad (A.3)$$

$$z = \left(\frac{t - t_h}{t} \right)^{1/2}$$

Golden-section search with the inequality (A.3) can cause numerical underflow when computing $f(h)$ near the right endpoint of the search interval. In lieu of Golden-section search, the inverse for the cooling section is computed using Nelder-Mead

590   optimization with the inequality (A.3) used as a Box constraint (Box, 1965).

595

600

Geoscientific
Instrumentation
Methods and
Data Systems

Discussions

605

8. Appendix B

ACRONYMS

HPP	Heat Pulse Probe
DP	Dual Probe
SP	Single Probe
PID	Proportional–Integral Derivative controller
DAC	Digital-to-Analog Converter
ADC	Analog-to-Digital Converter
AFE	Analog Front End
SDRAM	Synchronous dynamic random-access memory
DC	Direct Current
PLL	Phase-locked Loop
M2M	Machine-to-Machine
USB	Universal Serial Bus
RS-232	Recommended Standard 232 serial port
SDI-12	Serial Digital Interface at 1200 baud
PVC	Polyvinyl chloride
RMSD	Root-Mean Squared Difference
MB	Mean Bias
PD	Percentage Difference

Geoscientific
Instrumentation
Methods and
Data Systems

Discussions

EGU

Open Access

COTS	Commercial off-the-shelf
PCB	Printed Circuit Board
NA	Not Applicable

630

SYMBOLS AND SI UNITS

t	Time (s)
$\Delta\Gamma(t),\ \Delta T(t)$	Changes in temperature (K) as a function of time
q	Energy transfer per time per length of heater needle ($W\ m^{-1}$)
k	Thermal conductivity ($W\ m^{-1}\ K^{-1}$)
π	≈ 3.14159
$\{B, C, D\}$	Coefficients used for the SP model
r_n	Radius of heater needle (m)
α	Thermal diffusivity of soil ($m^2\ s^{-1}$)
$\log(\ )$	Natural logarithm function
t_0	Start time of heating Nichrome wire (s)
t_h	Stop time of heating Nichrome wire (s)
$t_T = t_i + t_h + t_c$	Total time of experiment (s)
t_i	Time used to determine initial temperature (s)
t_c	Time of cooling (s)
$r(t)$	Effective DP radius as function of time (m)
r	DP radius (m)
$r_{initial}$	Initial DP radius (m)
$d\ /\ dt$	Time derivative

635

640

645

650	H	$r^2 / 4\alpha$
	t_d	Time at which curve is assumed to be linear (s)
	$\gamma(r,t)$ or $\gamma(r(t),t)$	Signal processing computation step
	i	Integer index
	a_i	$\log(r(t_i))$
655	f_s	Sampling rate (Hz)
	Δt	$= 1/f_s$ as the timestep (s)
	$E_i(x)$	Exponential integral function
	ρ	Density ($\mathrm{kg\ m^{-3}}$)
	c	Specific heat capacity ($\mathrm{J\ kg^{-1}\ K^{-1}}$)
660	t_p	Time at which curve is at a maximum peak (s)
	t_a	Additional time delay (s)
	$\| \ \|$	Absolute value function
	x, y, z	Real numbers
	$f(x, y)$	Function of x, y
665	C_h	Volumetric heat capacity ($\mathrm{J\ m^{-3}\ K^{-1}}$)
	$\{C_m, C_o, C_w\}$	Volumetric heat capacity (mineral, organic and water)
	$\{\theta_m, \theta_o, \theta_w\}$	Volume fractions (mineral, organic and water)
	$\{c_m, c_o\}$	Specific heat capacity (mineral, organic) ($\mathrm{J\ kg^{-1}\ K^{-1}}$)
	$\{\rho_m, \rho_o\}$	Densities (mineral, organic) ($\mathrm{kg\ m^{-3}}$)
670	P	Electrical power (W)

Geoscientific
Instrumentation
Methods and
Data Systems

Discussions

Open Access

EGU

R_w	Resistance of Nichrome heater wire (ohms)
ℓ	Length of heater needle (m)
ΔE	Voltage drop over resistive element (V)
R_s	Resistance of sensor resistor (ohms)
I	Current through Nichrome heater wire (A)
E_{kn}	Known (measured) output voltage (V)
x_i	Real number with index i
$\hat{x}_i$	Comparison value as real number with index i
N	Index number as integer

675

9. Author Contributions

Conceptualization, N.K., B.C. and J.P.; methodology, N.K and B.C.; software, N.K.; validation, N.K. and B.C.; formal analysis, N.K.; investigation, N.K. and B.C.; resources, B.C. and J.P.; data curation, N.K.; writing—original draft preparation, N.K.; writing—review and editing, N.K., J.P. and B.C; visualization, N.K.; supervision, N.K., B.C. and J.P.; project administration, N.K., J.P. and B.C.; funding acquisition, J.P. and B.C.

680

10. Competing Interests

The authors declare that they have no conflict of interest.

685

11. Acknowledgements

690

Geoscientific
Instrumentation
Methods and
Data Systems
Discussions

12. References

695

Abramowitz, M. and Stegun, I. A.: Handbook of mathematical functions with formulas, graphs, and mathematical tables, Courier Dover Publications., 1964.

Abu-Hamdeh, N. H.: Measurement of the thermal conductivity of sandy loam and clay loam soils using single and dual probes, Journal of Agricultural Engineering Research, 80(2), 209–216, doi:10.1006/jaer.2001.0730, 2001.

700   Abu-Hamdeh, N. H. and Reeder, R. C.: Soil thermal conductivity: effects of density, moisture, salt concentration, and organic matter, Soil Science Society of America Journal, 64(4), 1285, doi:10.2136/sssaj2000.6441285x, 2000.

Ang, K. H., Chong, G. and Li, Y.: PID control system analysis, design, and technology, IEEE Transactions on Control Systems Technology, 13(4), 559–576, doi:10.1109/TCST.2005.847331, 2005.

Basinger, J. M., Kluitenberg, G. J., Ham, J. M., Frank, J. M., Barnes, P. L. and Kirkham, M. B.: Laboratory evaluation of the 705   dual-probe heat-pulse method for measuring soil water content, Vadose Zone Journal, 2(3), 389–399, doi:10.2113/2.3.389, 2003.

Blackwell, J. H.: A transient-flow method for determination of thermal constants of insulating material in bulk, Journal of Applied Physics, 25(2), 137–144, 1954.

Box, M. J.: A new method of constrained optimization and a comparison with other methods, The Computer Journal, 8(1), 710   42–52, doi:10.1093/comjnl/8.1.42, 1965.

Bristow, K. L.: Measurement of thermal properties and water content of unsaturated sandy soil using dual-probe heat-pulse probes, Agricultural and Forest Meteorology, 89(2), 75–84, doi:10.1016/S0168-1923(97)00065-8, 1998.

Bristow, K. L., Campbell, G. S. and Calissendorff, K.: Test of a Heat-Pulse Probe for Measuring Changes in Soil Water Content, Soil Science Society of America Journal, 57(4), 930, doi:10.2136/sssaj1993.03615995005700040008x, 1993.

715   Bristow, K. L., White, R. D. and Kluitenberg, G. J.: Comparison of single and dual probes for measuring soil thermal properties with transient heating, Australian Journal of Soil Research, 32, 447–464, 1994.

Bristow, K. L., Kluitenberg, G. J., Goding, C. J. and Fitzgerald, T. S.: A small multi-needle probe for measuring soil thermal properties, water content and electrical conductivity, Computers and Electronics in Agriculture, 31(3), 265–280, doi:10.1016/S0168-1699(00)00186-1, 2001.

720   Campbell, G. S., Calissendorff, C. and Williams, J. H.: Probe for measuring soil specific heat using a heat-pulse method, Soil Science Society of America Journal, 55(1), 291–293, 1991.

Carter, B. C., Vershinin, M. and Gross, S. P.: A comparison of step-detection methods: how well can you do?, Biophys J, 94(1), 306–319, doi:10.1529/biophysj.107.110601, 2008.

De Vries, D. A.: A nonstationary method for determining thermal conductivity of soil in situ, Soil Science, 73(2), 83–89, 1952.

725   Dias, P. C., Roque, W., Ferreira, E. C. and Siqueira Dias, J. A.: A high sensitivity single-probe heat pulse soil moisture sensor based on a single NPN junction transistor, Computers and Electronics in Agriculture, 96, 139–147, doi:10.1016/j.compag.2013.05.003, 2013.

Ebdon, D.: Statistics in Geography: a practical approach - revised with 17 programs, 2nd ed., Wiley-Blackwell., 1991.

Geoscientific
Instrumentation
Methods and
Data Systems
Discussions
Open Access
EGU

Green, S., Clothier, B. and Jardine, B.: Theory and Practical Application of Heat Pulse to Measure Sap Flow, Agronomy
730   Journal, 95(6), 1371, doi:10.2134/agronj2003.1371, 2003.

Ham, J. M. and Benson, E. J.: On the construction and calibration of dual-probe heat capcity sensors, Soil Science Society of
America Journal, 68, 1185–1190, 2004.

Hamming, R. W.: Digital Filters, 2nd ed., Prentice-Hall, Englewood Cliffs, N.J., 1983.

He, H., Dyck, M. F., Horton, R., Ren, T., Bristow, K. L., Lv, J. and Si, B.: Development and Application of the Heat Pulse
735   Method for Soil Physical Measurements, Reviews of Geophysics, doi:10.1029/2017RG000584, 2018.

Heitman, J. L., Basinger, J. M., Kluitenberg, G. J., Ham, J. M., Frank, J. M. and Barnes, P. L.: Field evaluation of the dual-
probe heat-pulse method for measuring soil water content, Vadose Zone Journal, 2(4), 552–560, doi:10.2113/2.4.552, 2003.

Hopmans, J. W., Šimunek, J. and Bristow, K. L.: Indirect estimation of soil thermal properties and water flux using heat pulse
probe   measurements: Geometry   and   dispersion   effects,   Water   Resources   Research,   38(1),   7-1-7–14,
740   doi:10.1029/2000WR000071, 2002.

Jin, H., Wang, Y., Zheng, Q., Liu, H. and Chadwick, E.: Experimental study and modelling of the thermal conductivity of
sandy soils of different porosities and water contents, Applied Sciences, 7(2), 119, doi:10.3390/app7020119, 2017.

Kamai, T., Tuli, A., Kluitenberg, G. J. and Hopmans, J. W.: Soil water flux density measurements near 1 cm/d using an
improved heat pulse probe design, Water Resour. Res., 44(4), W00D14, doi:10.1029/2008WR007036, 2008.

745   Kiefer, J.: Sequential Minimax Search for a Maximum, Proceedings of the American Mathematical Society, 4(3), 502–506,
doi:10.2307/2032161, 1953.

Kinar, N. J. and Pomeroy, J. W.: Measurement of the physical properties of the snowpack, Reviews of Geophysics, 53(2),
481–544, doi:10.1002/2015RG000481, 2015.

Kluitenberg, G. J.: Heat Capacity and Specific Heat, in Methods of Soil Analysis: Part 4 - Physical Methods, pp. 1201–1208,
750   Soil Science Society of America, Wisconsin, USA., 2002.

Kluitenberg, G. J., Ham, J. M. and Bristow, K. L.: Error analysis of the heat pulse method for measuring soil volumetric heat
capacity, Soil Science Society of America Journal, 57, 1444–1451, 1993.

Kluitenberg, G. J., Das, B. S. and Bristow, K. L.: Error analysis of heat pulse method for measuring soil heat capacity,
diffusivity,   and   conductivity,   Soil   Science   Society   of   America   Journal,   59(3),   719,
755   doi:10.2136/sssaj1995.03615995005900030013x, 1995.

Kluitenberg, G. J., Kamai, T., Vrugt, J. A. and Hopmans, J. W.: Effect of probe deflection on dual-probe heat-pulse thermal
conductivity measurements, Soil Science Society of America Journal, 74(5), 1537, doi:10.2136/sssaj2010.0016N, 2010.

Li, M., Si, B. C., Hu, W. and Dyck, M.: Single-probe heat pulse method for soil water content determination: comparison of
methods, Vadose Zone Journal, 15(7), 0, doi:10.2136/vzj2016.01.0004, 2016.

760   Liu, G. and Si, B.: Soil ice content measurement using a heat pulse probe method, Canadian Journal of Soil Science, 91(2),
235–246, doi:10.4141/cjss09120, 2011.

Liu, G. and Si, B. C.: Dual-probe heat pulse method for snow density and thermal properties measurement, Geophysical Research Letters, 35, 1–5, 2008.

765 Liu, G. and Si, B. C.: Errors analysis of heat pulse probe methods: experiments and simulations, Soil Science Society of America Journal, 74(3), 797–803, 2010.

Liu, G., Li, B., Ren, T. and Horton, R.: Analytical solution of the heat pulse method in a parallelepiped sample space, Soil Science Society of America Journal, 71(5), 1607–1619, 2007.

Liu, G., Wen, M., Chang, X., Ren, T. and Horton, R.: A self-calibrated dual probe heat pulse sensor for in situ calibrating the probe spacing, Soil Science Society of America Journal, 77(2), 417, doi:10.2136/sssaj2012.0434n, 2013.

770 Liu, G., Wen, M., Ren, R., Si, B., Horton, R. and Hu, K.: A general in situ probe spacing correction method for dual probe heat pulse sensor, Agricultural and Forest Meteorology, 226–227, 50–56, doi:10.1016/j.agrformet.2016.05.011, 2016.

Miner, G. L., Ham, J. M. and Kluitenberg, G. J.: A heat-pulse method for measuring sap flow in corn and sunflower using 3D-printed sensor bodies and low-cost electronics, Agricultural and Forest Meteorology, 246, 86–97, doi:10.1016/j.agrformet.2017.06.012, 2017.

775 Mori, Y., Hopmans, J. W., Mortensen, A. P. and Kluitenberg, G. J.: Multi-functional heat pulse probe for the simultaneous measurement of soil water content, solute concentration, and heat transport parameters, Vadose Zone Journal, 2(4), 561–571, doi:10.2113/2.4.561, 2003.

Morin, S., Domine, F., Arnaud, L. and Picard, G.: In-situ monitoring of the time evolution of the effective thermal conductivity of snow, Cold Regions Science and Technology, 64(2), 73–80, doi:10.1016/j.coldregions.2010.02.008, 2010.

780 Ochsner, T. E. and Baker, J. M.: In situ monitoring of soil thermal properties and heat flux during freezing and thawing, Soil Science Society of America Journal, 72(4), 1025, doi:10.2136/sssaj2007.0283, 2008.

Ochsner, T. E., Horton, R. and Ren, T.: A new perspective on soil thermal properties, Soil Science Society of America Journal, 65(6), 1641–1647, doi:10.2136/sssaj2001.1641, 2001.

Oppenheim, A., Kopec, G. and Tribolet, J.: Signal analysis by homomorphic prediction, IEEE Transactions on Acoustics, 785 Speech and Signal Processing, 24(4), 327–332, doi:10.1109/TASSP.1976.1162828, 1976.

Pearsall, K. R., Williams, L. E., Castorani, S., Bleby, T. M. and McElrone, A. J.: Evaluating the potential of a novel dual heat-pulse sensor to measure volumetric water use in grapevines under a range of flow conditions, Functional Plant Biology, 41(8), 874, doi:10.1071/FP13156, 2014.

Penner, E.: Thermal conductivity of frozen soils, Canadian Journal of Earth Sciences, 7(3), 982–987, doi:10.1139/e70-091, 790 1970.

Ramires, M. L. V., Nieto de Castro, C. A., Nagasaka, Y., Nagashima, A., Assael, M. J. and Wakeham, W. A.: Standard Reference Data for the Thermal Conductivity of Water, J. Phys. Chem. Ref. Data, 24(3), 1377, doi:10.1063/1.555963, 1995.

Ravazzani, G.: Open hardware portable dual-probe heat-pulse sensor for measuring soil thermal properties and water content, Computers and Electronics in Agriculture, 133, 9–14, doi:10.1016/j.compag.2016.12.012, 2017.

795 Saito, H., Šimůnek, J. and Mohanty, B. P.: Numerical analysis of coupled water, vapor, and heat transport in the vadose zone, Vadose Zone Journal, 5(2), 784–800, doi:10.2136/vzj2006.0007, 2006.

Saito, H., Šimůnek, J., Hopmans, J. W. and Tuli, A.: Numerical evaluation of alternative heat pulse probe designs and analyses, Water Resour. Res., 43(7), W07408, doi:10.1029/2006WR005320, 2007.

800 Sherfy, A. C., Lee, J., Tyner, J. S. and Kim, Y.: Improved Calibration for Estimating Soil Properties with a Multifunctional Heat Pulse Probe, Communications in Soil Science and Plant Analysis, 47(3), 305–312, doi:10.1080/00103624.2015.1123266, 2016.

Song, Y., Ham, J. M., Kirkham, M. B. and Kluitenberg, G. J.: Measuring soil water content under turfgrass using the dual-probe heat-pulse technique, Journal of the American Horticultural Society, 123(5), 937–941, 1998.

Steinhart, J. S. and Hart, S. R.: Calibration curves for thermistors, Deep Sea Research and Oceanographic Abstracts, 15(4), 805 497–503, doi:10.1016/0011-7471(68)90057-0, 1968.

Sturm, M. and Johnson, J. B.: Thermal conductivity measurements of depth hoar, Journal of Geophysical Research, 97, 2129–2139, 1992.

Trautz, A. C., Smits, K. M., Schulte, P. and Illangasekare, T. H.: Sensible heat balance and heat-pulse method applicability to in situ soil-water evaporation, Vadose Zone Journal, 13(1), 0, doi:10.2136/vzj2012.0215, 2014.

810 Valente, A., Morais, R., Tuli, A., Hopmans, J. W. and Kluitenberg, G. J.: Multi-functional probe for small-scale simultaneous measurements of soil thermal properties, water content, and electrical conductivity, Sensors and Actuators A: Physical, 132(1), 70–77, doi:10.1016/j.sna.2006.05.010, 2006.

Van Wijk, W. R. and De Vries, D. A.: Periodic temperature variations in a homogeneous soil, in Physics of Soil Environment, pp. 102–143, North-Holland Publishing Company, Amsterdam., 1963.

815 Wagner, W. and Pruß, A.: The IAPWS Formulation 1995 for the Thermodynamic Properties of Ordinary Water Substance for General and Scientific Use, Journal of Physical and Chemical Reference Data, 31(2), 387–535, doi:10.1063/1.1461829, 2002.

Wang, Q., Ochsner, T. E. and Horton, R.: Mathematical analysis of heat pulse signals for soil water flux determination, Water Resour. Res., 38(6), 27–1, doi:10.1029/2001WR001089, 2002.

Wen, M., Liu, G., Li, B., Si, B. C. and Horton, R.: Evaluation of a self-correcting dual probe heat pulse sensor, Agricultural 820 and Forest Meteorology, 200, 203–208, doi:10.1016/j.agrformet.2014.09.022, 2015.

Yang, C. and Jones, S. B.: INV-WATFLX, a code for simultaneous estimation of soil properties and planar vector water flux from fully or partly functioning needles of a penta-needle heat-pulse probe, Computers & Geosciences, 35(11), 2250–2258, doi:10.1016/j.cageo.2009.04.005, 2009.

Young, M. H., Campbell, G. S. and Yin, J.: Correcting dual-probe heat-pulse readings for changes in ambient temperature, 825 Vadose Zone Journal, 7(1), 22–30, doi:10.2136/vzj2007.0015, 2008.

Yun, T. S. and Santamarina, J. C.: Fundamental study of thermal conduction in dry soils, Granular Matter, 10(3), 197, doi:10.1007/s10035-007-0051-5, 2008.

Zhang, X., Heitman, J., Horton, R. and Ren, T.: Measuring near-surface soil thermal properties with the heat-pulse method: correction of ambient temperature and soil–air interface effects, Soil Science Society of America Journal, 78(5), 1575, 830 doi:10.2136/sssaj2014.01.0014, 2014.

Zhang, Y., Treberg, M. and Carey, S. K.: Evaluation of the heat pulse probe method for determining frozen soil moisture content, Water Resources Research, 47(5), doi:10.1029/2010WR010085, 2011.
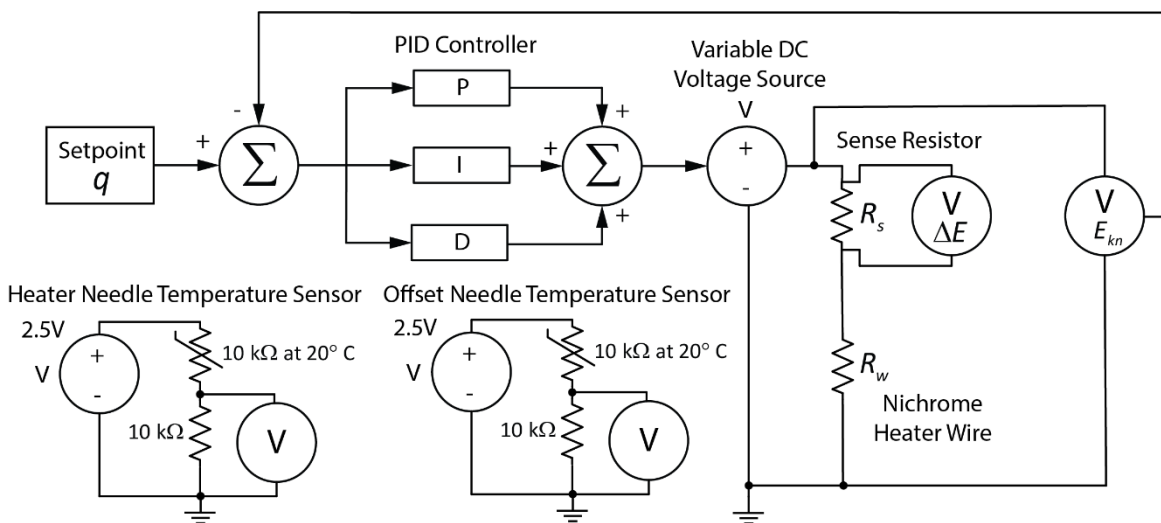
835

13. Figures

Figure 1: Conceptual block diagram of the HPP system. The setpoint q and the PID controller ensure a constant input of
840   heat into the soil over the length of the heater needle. The PID controller modulates heat inputs by changing the output of a variable DC voltage source and the feedback path is shown. A Kelvin-connection sense resistor measures the current through the Nichrome heater wire. A reduction in voltage over the sense resistor element is ΔE and the ground-referenced output voltage through the Nichrome wire is E_{kn}. The heater needle temperature sensor and offset needle temperature sensor circuits are also shown. A constant voltage source of 2.5V is connected to a half-bridge. One element of the bridge is a thermistor
845   with a nominal resistance of $10\,\mathrm{k\Omega}$ specified at a temperature of 20° C and the other is a precision resistor with a fixed resistance.

850

855

860
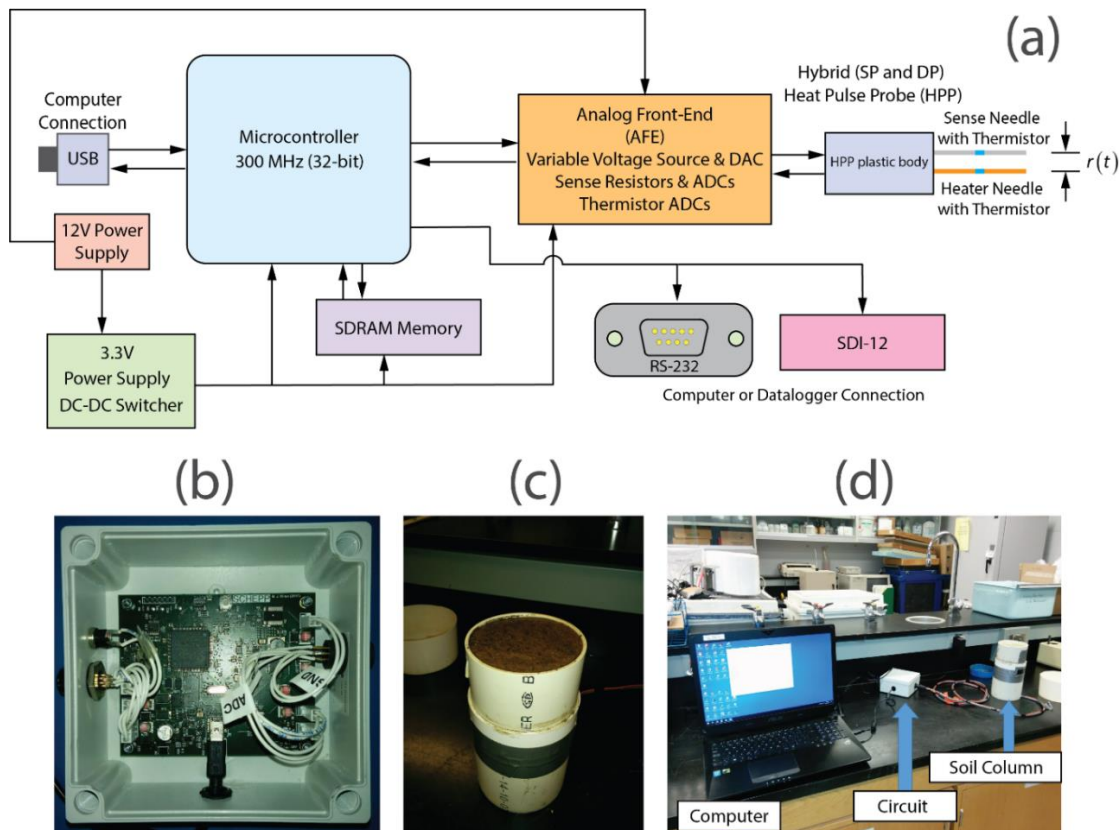
Figure 2: Diagrams showing system and microcontroller. (a) The circuit operation is controlled by a 32-bit microcontroller clocked at 300 MHz by a PLL. The microcontroller and associated transceiver circuity implement M2M communications where data and system operation can be exchanged between machines using commands sent over USB, RS-232, or SDI-12. The microcontroller acts as a state machine that samples data from the AFE and stores the data in SDRAM where signal

865 processing is conducted. The circuit is powered by a nominal 12V DC supply that is reduced to 3.3V by a DC-DC switcher. The HPP is a hybrid SP and DP design comprised of a heater needle and a sense needle. The effective distance between the needles as a function of time is $r(t)$. (b) Picture of circuit. (c) Soil column used in experiment. (d) Experimental setup.

Geoscientific
Instrumentation
Methods and
Data Systems
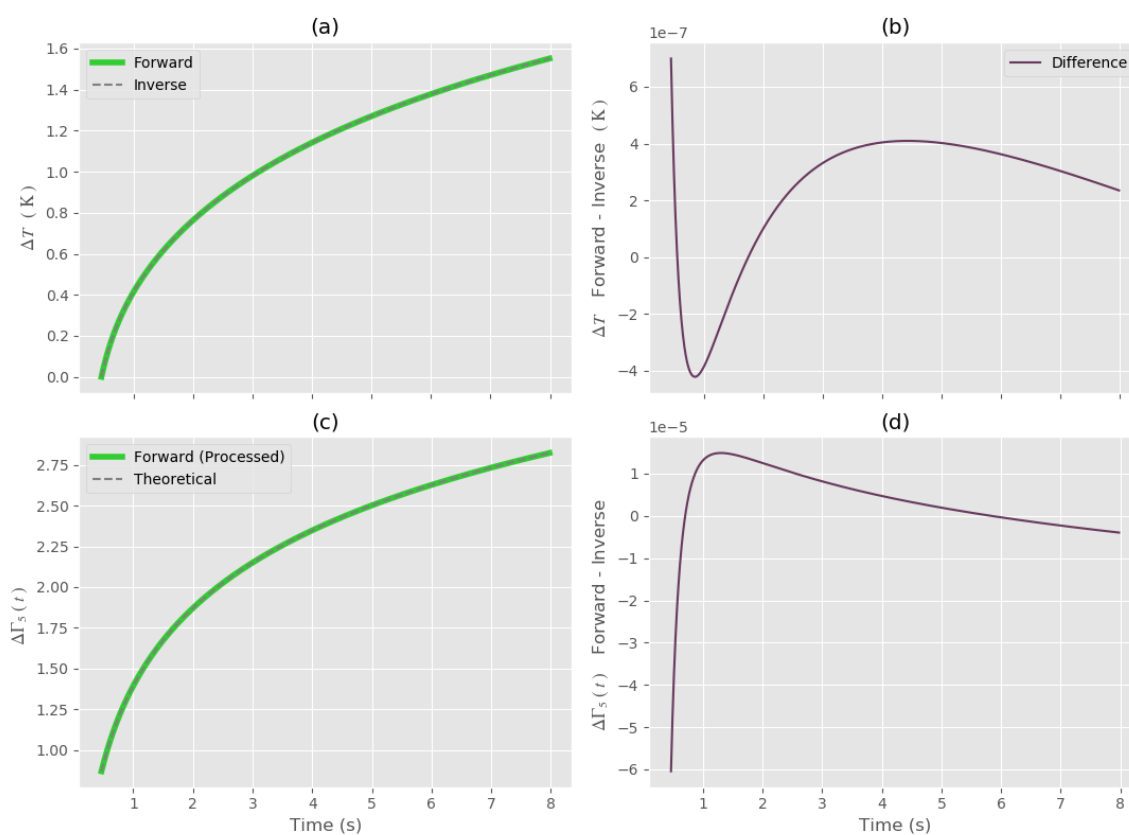
Discussions

870

875

Figure 3: Synthetic example of SP signal processing. (a) Forward model and reconstruction of the forward model by the inverse model. (b) Numerical difference between the forward and inverse models. (c) Forward model $\Delta\Gamma_5(t)$ from the signal processing compared to the theoretical model of $\Delta\Gamma_5(t)$. (d) Numerical difference between the forward model $\Delta\Gamma_5(t)$ and the theoretical model.
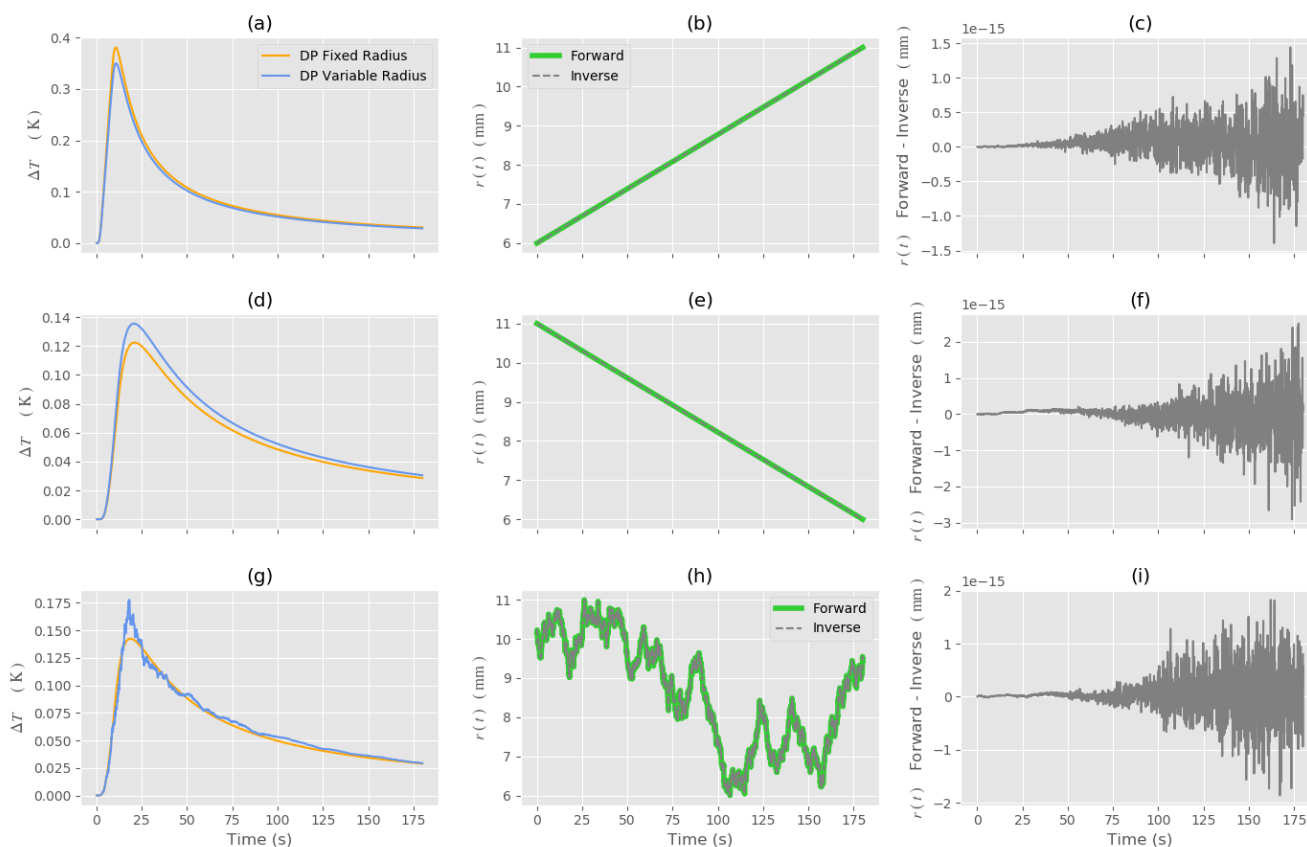
Figure 4: Synthetic example of DP forward and inverse models. (a), (d), (g) DP temperature change ΔT with a fixed and

885 variable radius. (b), (e), (h) Known change in $r(t)$ as a variable radius. The forward and inverse model (reconstruction by

signal processing) is shown. (c), (f), (i) Numerical difference between the forward and inverse models. Each row of Fig. 4

corresponds to a numerical experiment with an associated change in $r(t)$ given in the second column.
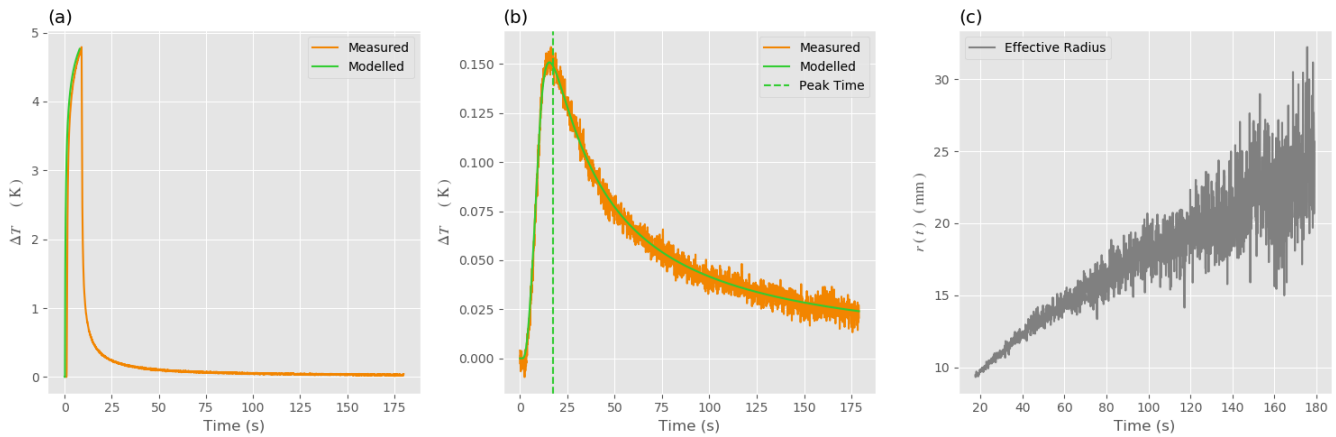
890

Figure 5: Example signal processing for sand showing (a) the measured and modelled SP heating curves; (b) the measured and modelled DP heating curves along with the detected peak time; (c) the detected change in effective radius $r(t)$ from the signal processing. The effective radius $r(t)$ as obtained from signal processing compensates for model, experimental error and physical changes in the spacing of the heater needles.

895

900

905

Geoscientific
Instrumentation
Methods and
Data Systems

Discussions

Figure 6: Example signal processing for peat showing (a) the measured and modelled SP heating curves; (b) the measured and modelled DP heating curves along with the detected peak time; (c) the detected change in effective radius $r(t)$ from the

910   signal processing. The effective radius $r(t)$ as obtained from signal processing compensates for model, experimental error and physical changes in the spacing of the heater needles.
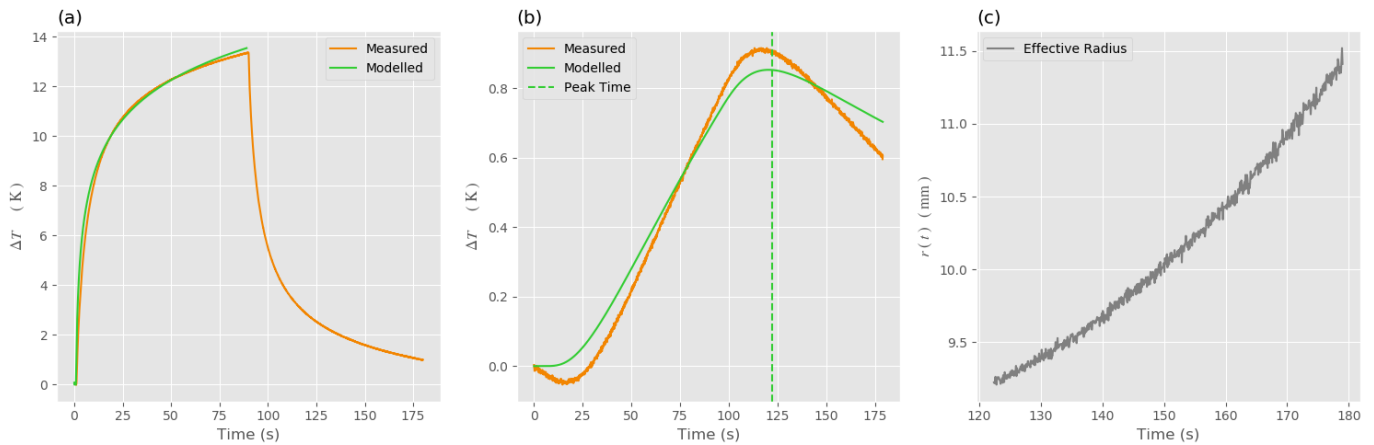
915

920
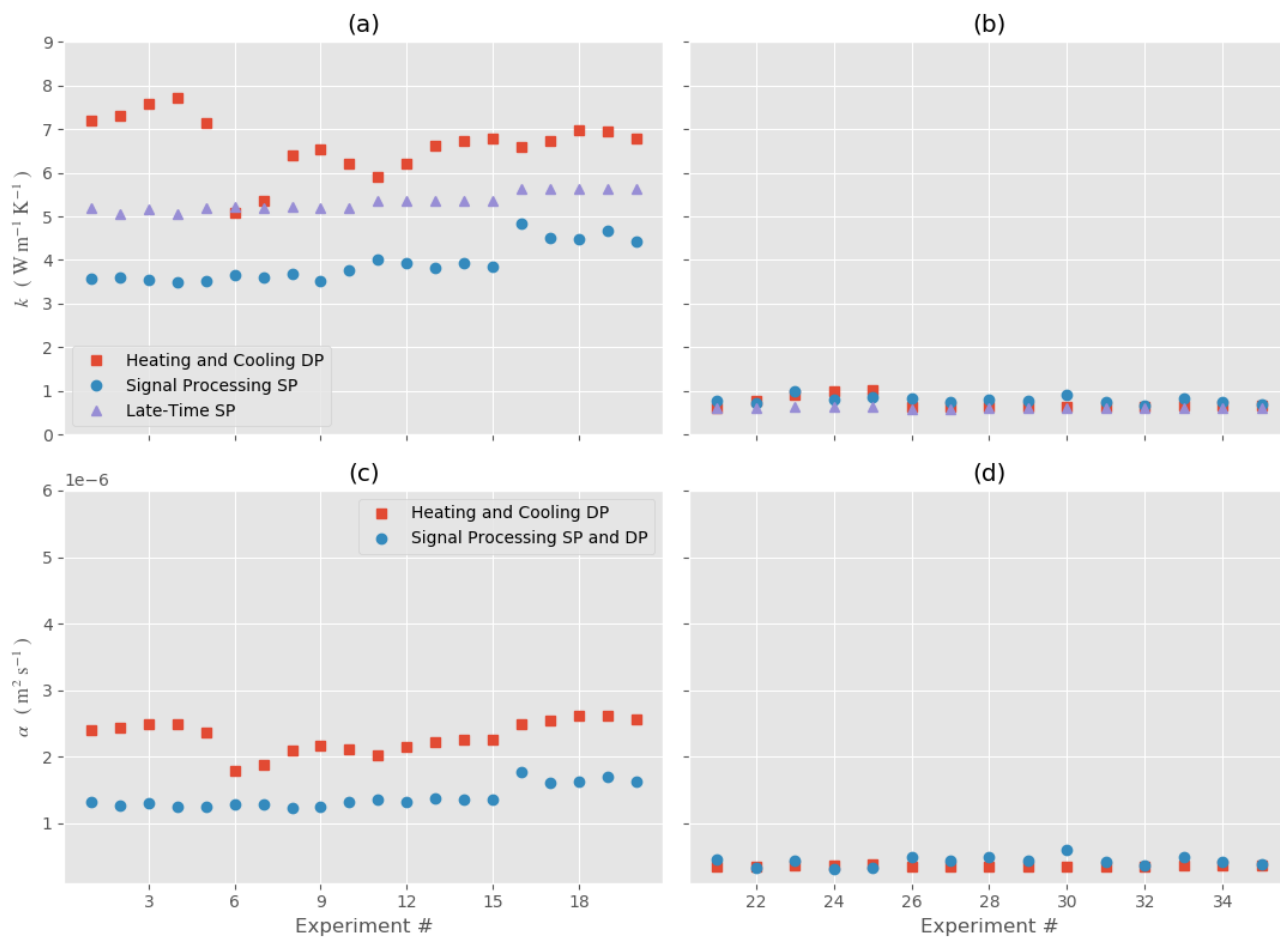
Figure 7: Thermal conductivity k and thermal diffusivity α for each of the experiments. (a) Thermal conductivity for sand. (b) Thermal conductivity for peat. (c) Thermal diffusivity for sand. (d) Thermal diffusivity for peat.

Geoscientific
Instrumentation
Methods and
Data Systems
Discussions
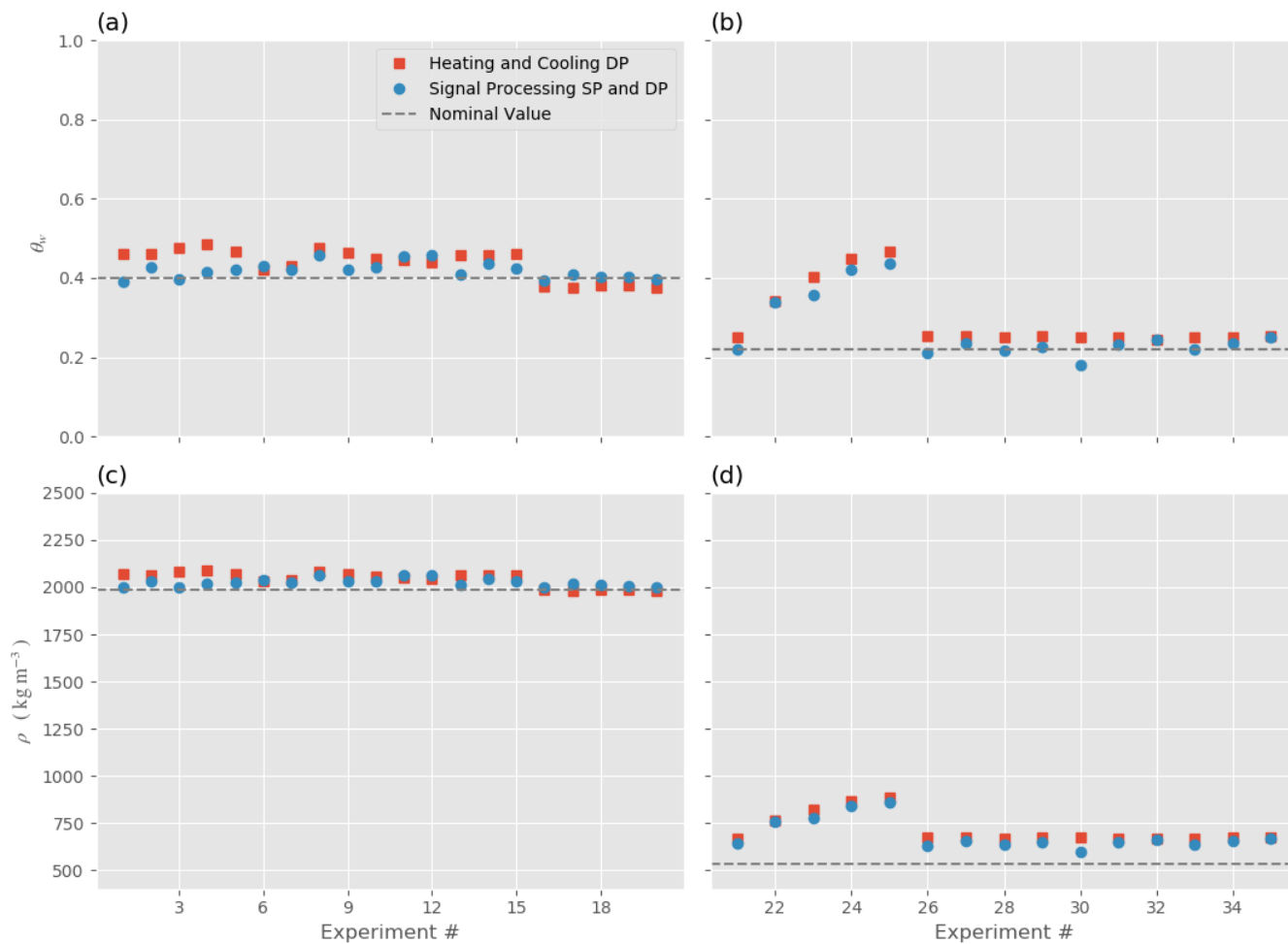
925

Figure 8: Water content θ_w and density ρ for each of the experiments. (a) Water content for sand. (b) Water content for peat. (c) Density for sand. (d) Density for peat.

Geoscientific
Instrumentation
Methods and
Data Systems

Open Access

EGU

Discussions
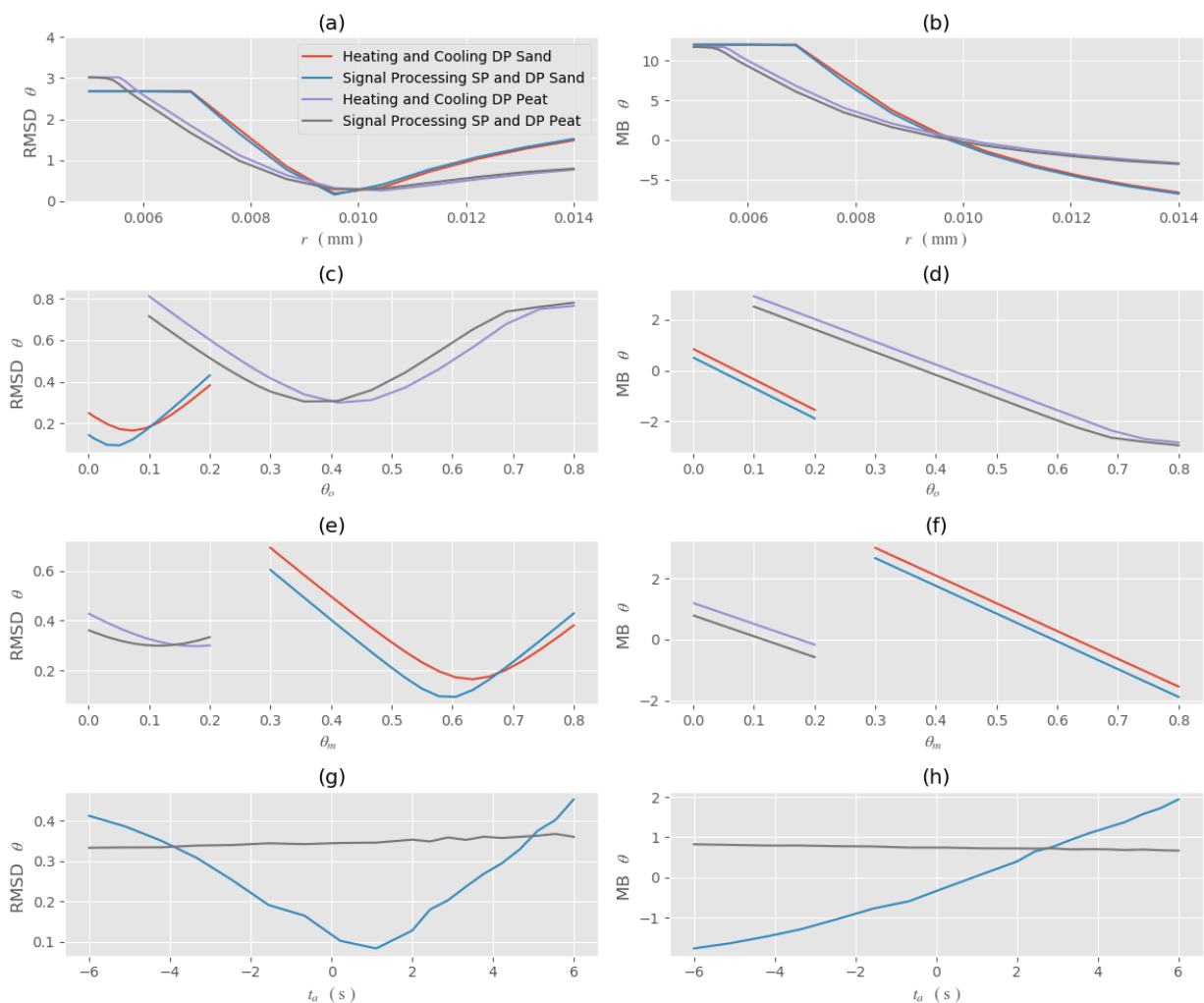
930

Figure 9: Sensitivity analysis for water content θ_w for sand and peat with respect to the different models. (a) RMSD for changes in the calibrated initial radius r. (b) MB for changes in the calibrated initial radius. (c) RMSD for changes in the organic volume fraction θ_o. (d) MB for changes in the organic volume fraction θ_o. (e) RMSD for changes in the mineral volume fraction θ_m. (f) MB for changes in the mineral volume fraction θ_m. (g) RMSD for changes in the time delay t_a. (h)

935 MB for changes in the time delay t_a.
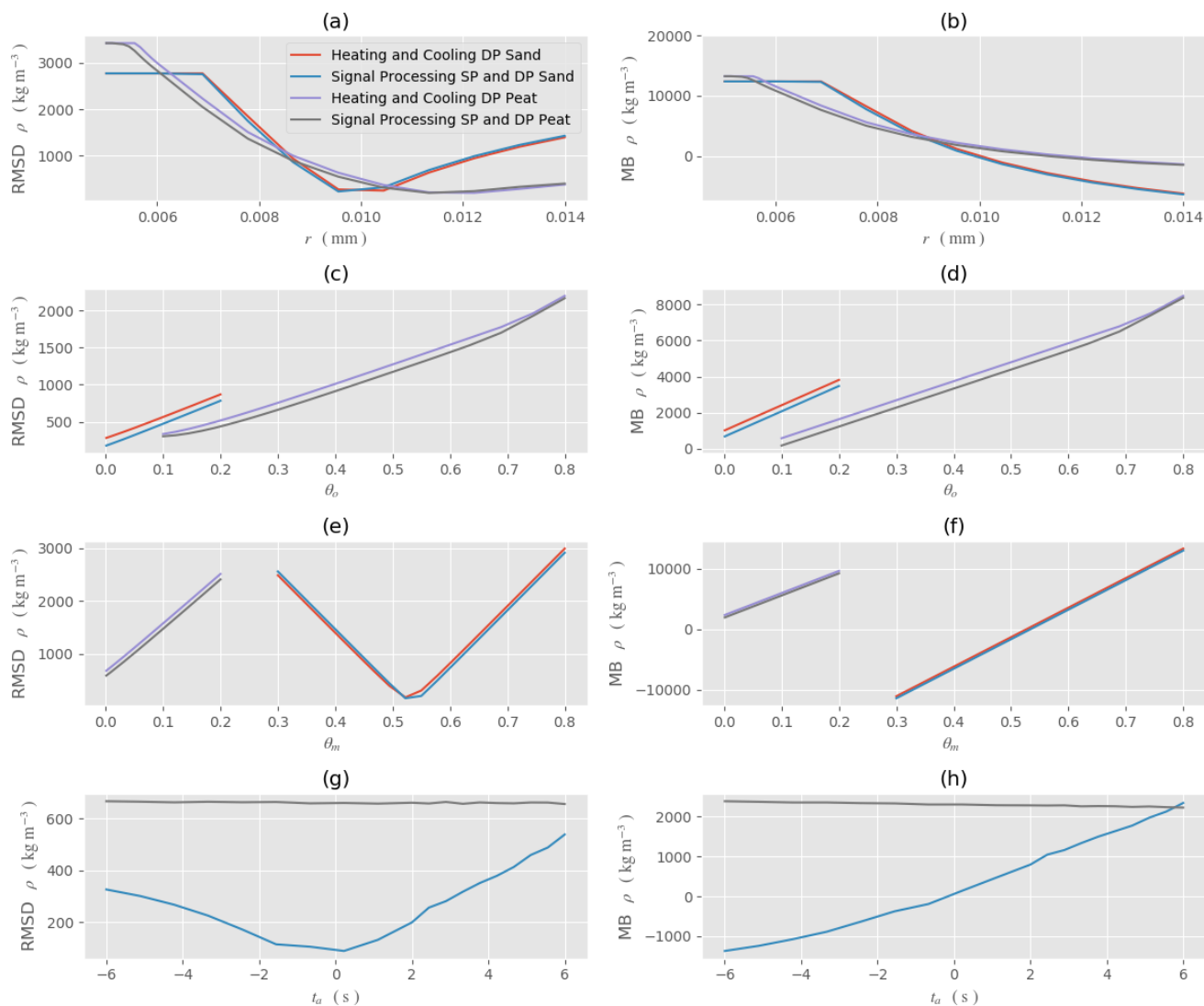
Figure 10: Sensitivity analysis for density ρ for sand and peat with respect to the different models. (a) RMSD for changes in the calibrated initial radius r. (b) MB for changes in the calibrated initial radius. (c) RMSD for changes in the organic volume fraction θ_o. (d) MB for changes in the organic volume fraction θ_o. (e) RMSD for changes in the mineral volume fraction θ_m. (f) MB for changes in the mineral volume fraction θ_m. (g) RMSD for changes in the time delay t_a. (h) MB for changes in the time delay t_a.

Sand	Description
$\rho = 1987 \ \mathrm{kg \ m^{-3}}$	Total density of sand and water mixture
$\theta_w = 0.40$	Volumetric water content
$\theta_o = \dfrac{M_0 m_T}{\rho_o V_T} = 9.2 \times 10^{-3} = 0.92\%$	Maximum fraction of organic content $M_0 = 7.5 \times 10^{-3} = $ Organic mass fraction from incineration $m_T = 1.31 \ \mathrm{kg} = $ Total mass of soil (kg) $\rho_0 = 1300 \ \mathrm{kg \ m^{-3}} = $ Density of soil organic matter (kg m^{-3}) $V_T = 8.25 \times 10^{-4} \ \mathrm{m^3} = $ Total volume (m^3)
$\theta_m = 0.55$	Volumetric mineral content of sand
$C_o = 2.5 \times 10^6 \ \mathrm{J \ m^{-3} \ K^{-1}}$	Volumetric heat capacity of organic content (Van Wijk and De Vries, 1963)
$C_m = 1.9 \times 10^6 \ \mathrm{J \ m^{-3} \ K^{-1}}$	Volumetric heat capacity of mineral content (Van Wijk and De Vries, 1963)

Peat	
$\rho = 535 \ \mathrm{kg \ m^{-3}}$	Total density of peat and water mixture
$\theta_w = 0.22$	Volumetric water content
$\theta_o = 0.30$	Organic matter fraction
$\theta_m = 0.01$	Volumetric mineral content
$C_o = 1.0 \times 10^6 \ \mathrm{J \ m^{-3} \ K^{-1}}$	Volumetric heat capacity of organic content
$C_m = 1.1 \times 10^6 \ \mathrm{J \ m^{-3} \ K^{-1}}$	Volumetric heat capacity of mineral content

950

Sand and Peat	
$\rho_o = 1300 \ \mathrm{kg \ m^{-3}}$	Density of organic matter
$\rho_m = 2900 \ \mathrm{kg \ m^{-3}}$	Density of mineral content from parent material

Table 1: Quantities utilized for sand and peat HPP experiments.

955

960

Trial Number for Sand	Experiment Identifier	Heat Pulse Strength (W m^{-1})	t_h Time of Heating	t_T Total Time of Experiment	Number of Repetitions	Days Between Last Trial	#
1	A	45	8 s	3 min	5	0	1-5
2	B	45	8 s	3 min	5	1	6-10
	C	45	11 s	3 min	5		11-15
	D	55	20 s	3 min	5		16-20

965

Trial Number for Peat							
1	E	20	89 s	3 min	5	0	21-25
2	F	20	89 s	3 min	5	1	26-30
3	G	20	89 s	3 min	5	1	31-35

970

975

Table 2: Heat pulse strengths, time of heating and cooling and total time for each experiment conducted on sand and peat. The experiment identifier is an alphabetical letter that identifies the experiment set. The # is an indication of the total number of experiments conducted per set.

980

985

990

995

1000

SP Model
$q = 45$ W m^{-1}
$k = 5.2$ W m^{-1} K^{-1}
$B = 0.016$
$C = 0.203$
$D = 0.402$

1005

DP Model
$q = 45$ W m^{-1}
$k = 5.2$ W m^{-1} K^{-1}
$\theta_m = 0.59$
$\theta_o = 9.2 \times 10^{-3}$
$\theta_w = 0.40$
6 mm $\leq r(t) \leq$ 11 mm

Table 3: Synthetic SP and DP model inputs.

1010

Quantity and Units	Signal Processing SP and DP	Heating and Cooling DP	Late-time SP
k $\left(\text{W m}^{-1}\text{ K}^{-1}\right)$	3.67	6.41	5.21
α $\left(\text{m}^2\text{ s}^{-1}\right)$	1.23×10^{-6}	2.09×10^{-6}	NA
θ_w	0.46	0.48	NA
ρ $\left(\text{kg m}^{-3}\right)$	2065	2083	NA

	PD for Signal Processing SP and DP (%)	Numerical Difference Signal Processing SP and DP	PD for Heating and Cooling DP (%)	Numerical Difference for Heating and Cooling DP
θ_w	-15	-0.06	-19	-0.08
ρ $\left(\text{kg m}^{-3}\right)$	-4	-78.3 kg m^{-3}	-5	-95.9 kg m^{-3}

Table 4: Comparisons for sand example.

1015

1020

1025

Quantity and Units	Signal Processing SP and DP	Heating and Cooling DP	Late-time SP
$k \ \left(\text{W m}^{-1} \ \text{K}^{-1}\right)$	0.81	0.99	0.64
$\alpha \ \left(\text{m}^2 \ \text{s}^{-1}\right)$	3.18×10^{-7}	3.73×10^{-7}	NA
θ_w	0.42	0.45	NA
$\rho \ \left(\text{kg m}^{-3}\right)$	841	868	NA

	PD for Signal Processing SP and DP (%)	Numerical Difference Signal Processing SP and DP	PD for Heating and Cooling DP (%)	Numerical Difference for Heating and Cooling DP
θ_w	-92	-0.202	-104	-0.2
$\rho \ \left(\text{kg m}^{-3}\right)$	-57.1	$-306 \ \text{kg m}^{-3}$	-62	$-333 \ \text{kg m}^{-3}$

Table 5: Comparisons for peat example.

1030

1035

1040

Soil Type and Experiment Identifier	#	θ_w RMSD Heating and Cooling DP	θ_w RMSD Signal Processing SP and DP	θ_w MB Heating and Cooling DP	θ_w MB Signal Processing SP and DP	θ_w PD Heating and Cooling DP	θ_w PD Signal Processing SP and DP
sand A	1-5	0.16	0.04	0.35	0.05	-17.4	-2.42
sand B	6-10	0.12	0.08	0.24	0.16	-11.9	-7.84
sand C	11-15	0.12	0.09	0.26	0.19	-12.9	-9.29
sand D	16-20	0.05	0.01	-0.11	0.0055	5.51	-0.275
peat E	21-25	0.4	0.35	0.81	0.67	-73.8	-61.3
peat F	26-30	0.07	0.04	0.16	-0.0298	-14.7	2.71
peat G	31-35	0.07	0.04	0.15	0.08	-14	-6.99
SAND ALL	NA	0.23	0.13	0.73	0.4	-9.18	-4.96
PEAT ALL	NA	0.42	0.35	1.13	0.72	-34.2	-21.9

Table 6: RMSD, MB, and PD comparisons for θ_w.

1045

1050

Geoscientific
Instrumentation
Methods and
Data Systems
Discussions

1055

Soil Type and Experiment Identifier	#	$\rho \ (\text{kg m}^{-3})$ RMSD Heating and Cooling DP	$\rho \ (\text{kg m}^{-3})$ RMSD Signal Processing SP and DP	$\rho \ (\text{kg m}^{-3})$ MB Heating and Cooling DP	$\rho \ (\text{kg m}^{-3})$ MB Signal Processing SP and DP	ρ PD (%) Heating and Cooling DP	ρ PD (%) Signal Processing SP and DP
sand A	1-5	201.24	73.4	447.41	148.1	-4.5	-1.49
sand B	6-10	157.97	118.88	338.58	256.63	-3.41	-2.58
sand C	11-15	161.04	134.66	357.81	285.62	-3.6	-2.87
sand D	16-20	7.5	48.52	-10.4	105.3	0.1	-1.06
peat E	21-25	621.55	561.12	1332.24	1193.97	-49.8	-44.6
peat F	26-30	305.03	223.27	682.06	490.22	-25.5	-18.3
peat G	31-35	301.43	267.96	673.84	596.93	-25.2	-22.3
SAND ALL	NA	302.4	200.02	1133.43	795.64	-2.85	-2
PEAT ALL	NA	755.13	660.69	2688.13	2281.12	-33.5	-28.4

Table 7: RMSD, MB, and PD comparisons for ρ.